

# NAVAL POSTGRADUATE SCHOOL MONTEREY, CALIFORNIA



## THESIS

**EXPERIMENTAL STUDY OF A DELAMINATED  
SANDWICH COMPOSITE SUBJECT TO IMPACT  
AND/OR COMPRESSIVE LOADING**

by

Larry A. Clawson, Jr.

June, 1995

Thesis Advisor:

Young W. Kwon

19980819 099

Approved for public release; distribution is unlimited.

DTIC QUALITY INSPECTED 1

REPORT DOCUMENTATION PAGE			Form Approved OMB No. 0704-0188	
Public reporting burden for this collection of information is estimated to average 1 hour per response, including the time for reviewing instruction, searching existing data sources, gathering and maintaining the data needed, and completing and reviewing the collection of information. Send comments regarding this burden estimate or any other aspect of this collection of information, including suggestions for reducing this burden, to Washington Headquarters Services, Directorate for Information Operations and Reports, 1215 Jefferson Davis Highway, Suite 1204, Arlington, VA 22202-4302, and to the Office of Management and Budget, Paperwork Reduction Project (0704-0188) Washington DC 20503.				
1. AGENCY USE ONLY	2. REPORT DATE June 1995.	3. REPORT TYPE AND DATES COVERED Master's Thesis		
4. TITLE AND SUBTITLE EXPERIMENTAL STUDY OF A DELAMINATED SANDWICH COMPOSITE SUBJECT TO IMPACT AND/OR COMPRESSION LOADING-		5. FUNDING NUMBERS		
6. AUTHOR(S) Clawson, Larry A., Jr				
7. PERFORMING ORGANIZATION NAME(S) AND ADDRESS(ES) Naval Postgraduate School Monterey CA 93943-5000		8. PERFORMING ORGANIZATION REPORT NUMBER		
9. SPONSORING/MONITORING AGENCY NAME(S) AND ADDRESS(ES)		10. SPONSORING/MONITORING AGENCY REPORT NUMBER		
11. SUPPLEMENTARY NOTES The views expressed in this thesis are those of the author and do not reflect the official policy or position of the Department of Defense or the U.S. Government.				
12a. DISTRIBUTION/AVAILABILITY STATEMENT Approved for public release; distribution is unlimited.		12b. DISTRIBUTION CODE		
13. ABSTRACT Symmetric sandwich composites are very attractive for use in various structural applications due to their low weight and high flexural stiffness. This research focuses on experimental studies of the damage tolerance of a sandwich composite with delamination subjected to low-energy impact and/or compressive loads. Tests are performed to correlate delamination length with failure loads and loss of damage tolerance. The impact force history is used to determine the work, kinetic energy and momentum imparted to the sample in order to gain an understanding of the mechanisms involved in damage due to impact.				
14. SUBJECT TERMS Symmetric sandwich composite, low-energy impact, delamination.		15. NUMBER OF PAGES 98		
		16. PRICE CODE		
17. SECURITY CLASSIFICATION OF REPORT Unclassified	18. SECURITY CLASSIFICATION OF THIS PAGE Unclassified	19. SECURITY CLASSIFICATION OF ABSTRACT Unclassified	20. LIMITATION OF ABSTRACT UL	

NSN 7540-01-280-5500

Standard Form 298 (Rev. 2-89)  
Prescribed by ANSI Std. Z39-18 298-102



Approved for public release; distribution is unlimited.

**EXPERIMENTAL STUDY OF A DELAMINATED SANDWICH  
COMPOSITE SUBJECT TO IMPACT AND/OR COMPRESSIVE  
LOADING**

Larry A. Clawson, Jr  
Lieutenant,, United States Navy  
B.S., University of Mississippi, 1985

Submitted in partial fulfillment  
of the requirements for the degree of

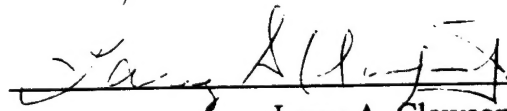
**MASTER OF SCIENCE IN MECHANICAL ENGINEERING**

from the

**NAVAL POSTGRADUATE SCHOOL**

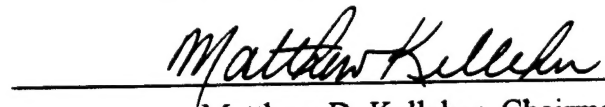
**June 1995**

Author:

  
Larry A. Clawson, Jr.

Approved by:

  
Dr. Young W. Kwon, Thesis Advisor

  
Matthew D. Kelleher, Chairman  
Department of Mechanical Engineering

17-2-2  
C506-2  
C. 2

# **ABSTRACT**

Symmetric sandwich composites are very attractive for use in various structural applications due to their low weight and high flexural stiffness. This research focuses on experimental studies of the damage tolerance of a sandwich composite with delamination subjected to low-energy impact and/or compressive loads. Tests are performed to correlate delamination length with failure loads and loss of damage tolerance. The impact force history is used to determine the work, kinetic energy and momentum imparted to the sample in order to gain an understanding of the mechanisms involved in damage due to impact.



## TABLE OF CONTENTS

I.	INTRODUCTION .....	1
II.	BACKGROUND .....	5
III.	EXPERIMENTAL PROCEDURES .....	11
	A. COMPRESSION TESTING .....	11
	B. IMPACT TESTING .....	14
IV.	EXPERIMENTAL RESULTS .....	21
	A. PRE-IMPACT COMPRESSION TEST RESULTS .....	21
	B. IMPACT TEST RESULTS .....	25
V.	CONCLUSIONS .....	45
	APPENDIX .....	47
	LIST OF REFERENCES .....	87
	INITIAL DISTRIBUTION LIST .....	89



## I. INTRODUCTION

To obtain weight reduction while maintaining the high flexural stiffness necessary in state-of-the-art aircraft airframe design, the aircraft and aviation industries are increasingly turning to sandwich composites for structural building materials. Many other industries are utilizing the strength to weight benefits of the sandwich composites as well; applications include the space shuttle program, remotely piloted vehicle (RPV) aircraft and small boats to name a few. Sandwich composite materials consist of two face plates adhesively bonded to a light-weight inner core. The faceplates carry the principle loads while the inner core acts to transmit the shear between the faceplates. Most recent focus on sandwich composite material selection has been on using graphite/epoxy or fiberglass/epoxy facesheets with various types of honeycomb or lightweight foam material for the core.

One of the major concerns in using the sandwich composites is the loss of load carrying capability that may be suffered in the event of delamination between the outer skins and the inner core. Delamination may occur due to a number of reasons such as low energy impact, manufacturing defects or high stress concentrations at geometric or material discontinuities. The delamination may occur

unknowingly and severely limit the load carrying capacity of the composite material. Knowledge of the damage tolerance of the material, with and without delamination, is necessary to allow engineers to determine what degree of impact, if any, can be allowed in the service life of the sandwich composite.

One method of assessing the damage tolerance or toughness of composite materials is through instrumented impact followed by determination of the residual ultimate compression strength [Ref. 1]. This study will assess the damage tolerance of various sizes of symmetric sandwich composite structural members. The term 'symmetric' refers to the fact that the two facesheets are of identical material and thickness. All material samples in this study have identical facesheets and the same type of inner core. The facesheets consist of a graphite epoxy ( $O_2/90_2/O_2$ ) composite while the core is Rohacell Polymethacrylimide rigid foam. Different samples, each having a different core thickness, are tested to determine the effect core thickness has on the damage tolerance of the sandwich composite. Furthermore, samples which have various lengths of delamination between the facesheet and core are tested to determine the effect of delamination on the damage

tolerance. The testing consists of edge-wise compression tests and instrumented low energy impact.

The primary focus of this work is an experimental study of the damage tolerance of a symmetric sandwich composite subjected to compressive and/or impact loading. The effect of composite delamination on the damage tolerance will be observed, and the impact force history will be used to develop energy, work and momentum equations to aid in understanding of the mechanisms involved in damage due to impact.



## II. BACKGROUND

Within the past decade much research on impact damage and response of composite materials has been conducted. Most of the work has centered on laminate composites, but sandwich composites have recently been a rapidly growing field of study. Most studies examine the failure modes, including delamination, of the composite material under inspection, but very little literature exists on studying the effects of pre-existing large scale delaminations such as those used in this study.

Work by Nemes and Simmonds [Ref. 2] has shown that, for impact conditions producing displacements larger than  $1/100$ th the face plate thickness, the contact deformations of fully intact sandwich composites are dominated by the deformations of the core rather than by the faceplate. The most prevalent observed damage of a foam core sandwich composite appears to occur at the bond layer between the facesheets and the foam core with the greatest damage occurring between the impacted facesheet and the core. They have shown that impact damage in the faceplate/core interface is dominantly driven by the excessive transverse shear stress resulting from the impact. Their work centered on developing a finite element program using linear elastic constitutive models for the facesheets and epoxy bond layer in conjunction with a foam constitutive model that included

nonlinear hardening plasticity and coupling between volumetric and deviatoric deformation. Using a transient finite-element code with four-noded uniform strain quadrilaterals, they numerically solve the equations for balance of mass and momentum. The program used five elements through the thickness of each faceplate, two elements through the thickness of each bond layer and 13 elements through the thickness of the foam core. The computations were performed on a CRAY X/MP and required nine hours of CPU time to run an impact simulation of 5 ms duration. The large computational time was the result of the small time steps required for numerical stability of the explicit integration. This large amount of computer time, even with a super-computer, is indicative of the complexity of the impact response and illustrates why most final confirming impact tests of a component are usually performed on the real structure.

Kim and Jun [Ref. 3] have shown that for laminated composite sandwich plates, the energy in a low energy impact that is not converted to elastic deformation is absorbed by the specimen as permanent deformation and damage such as matrix cracking, delamination between plies, fiber breakage and fiber matrix debonding. For sandwich composites additional, and more likely, damage includes core crushing and shear deformation. Observing the delamination

of monolithic laminates as compared to the facesheets of various types of sandwich plates, they found that delamination size increases rapidly from impact side to the farthest interply location and the largest delamination occurs at the farthest interply location for a laminate. The bending stresses due to impact are more severe at farther layers from the impacted face, and these stresses result in more severe matrix cracking and possible fiber breakage. It is believed the delamination damage process in monolithic laminates is caused by delamination propagation initiated by transverse matrix cracks [Ref. 4]. Since the sandwich structures have the additional energy absorbing mechanisms, core crushing and shear deformations, the sandwich laminated faceplates generally have much smaller deformation damage than that of a monolithic laminate with the same ply orientation. The difference is attributed to more energy being absorbed by core crushing and core shear deformations.

In a treatise on low-energy impact testing, Sjoblom, Hartness and Cordell [Ref. 5] point out that knowing the initial potential energy of the impactor in an impact test is not enough to predict the effect of an impact. The impacted specimen response depends on geometry, material properties, and velocity of the impactor. They report that using an impact load cell for the detection of damage works

very well as long as damage results in a fast, large load drop. Their work confirms that of Crane and Juska [Ref. 1] whereby the impact force history may be used to determine the force, displacement and energy at which major damage was initiated. By plotting energy loss of the impactor-vs-initial impact energy over a range of impact energies, Sjoblom, Hartness and Cordell found that damage by delamination in a given sample was reflected by an abrupt increase in impactor energy loss at a specific level of initial impact energy. Small matrix cracks were found in the samples which had been impacted with impact energies below those energy levels which resulted in delamination damage. They report four distinct stages in the damage process: 1) minor matrix damage, 2) delaminations, 3) backface damage and finally, 4) penetration.

Plastic deformation and small-scale matrix cracking cannot be detected by observing the force/time history. Carlyle and Adler [Ref. 6] have shown that acoustic emission sensors can be used to detect and measure the early onset of matrix cracking. In studies of delamination of laminated sandwich plates due to impact, most researchers use X-ray, C-scan, section microscopy or simple depley technique to measure the delamination.

In a study on increased fracture toughness of graphite-epoxy composites through intermittent interlaminar



debonding, Jea and Felbeck [Ref.7] have shown that an intermittent debond existing between plies of a graphite-epoxy composite can result in increased fracture energy while maintaining strength and stiffness. The phenomenon is caused by the low fracture strength of the debonded area effectively blunting and diverting internal cracks within a lamina. The blunting and diverting prevents the crack from propagating transversely into adjacent layers. Hwu and Hu [Ref. 8] have reported buckling loads of sandwich beams with small delaminations actually being higher than the buckling loads with no delamination.



### III. EXPERIMENTAL PROCEDURES

This section provides detailed descriptions, illustrations and procedures of the testing performed for this research. The tests performed were edge-wise compression and the low-energy impact tests.

#### A. COMPRESSION TESTING

All tests throughout this study were performed at the Naval Postgraduate School, Monterey, California, in an ambient temperature of  $68^{\circ} \text{ F} \pm 5^{\circ} \text{ F}$ . with an average relative humidity of to  $40\% \pm 8\%$ .

For the compressive buckling portion of this study either a 120,000 lb. Riehle Material Testing Machine or a 2,200 lb. Instron Universal Testing Machine was used to determine both the pre-impact and post-impact ultimate strength in compression. Special testing fixtures were designed and fabricated to ensure simply supported beam conditions existed on the loaded ends of the test specimen. The compression test specimen fixtures are shown in Figure 1. The unloaded surfaces of the test specimen were unconstrained while the loaded ends were aligned in the test fixtures with shims to ensure loading on the neutral axis. The cylindrical shafts of the test fixtures were free to rotate in the journal of the fixtures. The freedom of

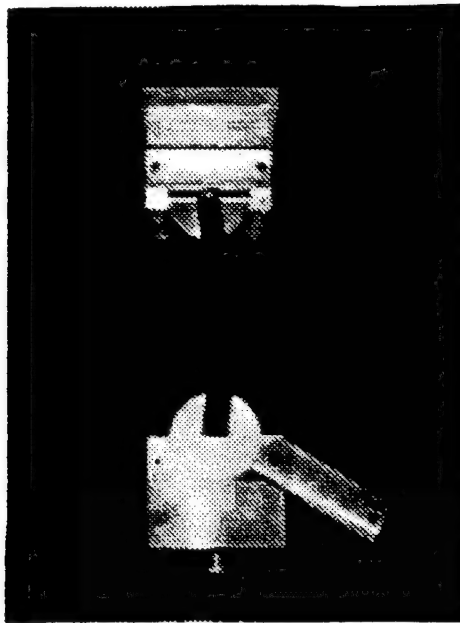


Figure 1. Compression Test Specimen Fixtures

rotation ensured the simply supported end conditions prevailed throughout the conduct of the compression test.

The material under observation throughout the length of this study is a symmetric sandwich composite with graphite-epoxy ( $O_2/90_2/O_2$ ) top and bottom skins and Rohacell Polymethacrylimide rigid foam inner core. All test specimens were 38.1 cm (15 in.) in length and 3.81 cm (1.5 in.) in width. The graphite-epoxy skins were nominally 0.096 cm (0.038 in.) thick. The specimen foam thickness was varied to observe the effect of inner-core thickness on ultimate strength in compression and toughness. Foam thicknesses of 0.30 cm (0.118 in.), 0.635 cm (0.25 in.), and 1.27 cm (0.5 in.) were used. Some samples were ordered from

the manufacturer with delamination between the skin and core. The samples with delamination were delaminated on one side only. The delamination ran across the total width of the test sample, and the longitudinal length of delamination varied from 1.27 cm (0.5 in.), 2.54 cm (1.0 in.), 5.08 cm (2.0 in.), 10.16 cm (4.0 in.), and 15.24 cm (6.0 in.). All delaminated samples had 0.635 cm (0.25 in) thick foam cores.

The test specimens were instrumented with 1.27 cm (0.5 in.) Measurements Group, Inc. CEA-13-250UN-350 precision strain gages mounted longitudinally and centered, one on each side. The gages had a gage factor of  $2.12 \pm 5\%$ . Gage outputs were connected to a Measurements Group SB-10 Switch and Balance Unit, and the strain readouts were provided by a Measurements Group P-3500 Strain Indicator. With the mounting fixtures installed on the compression test machine, the test specimen was fitted into the mounting fixtures and aligned with shims of various sizes. The center and axial deflections were measured with Sterrett dial indicators. Figure 2 illustrates the test specimen in the mounting fixtures for the typical, sans dial indicators, compression test setup.



Figure 2. Compression Test Setup

All compression tests were manually load controlled. The low speed loading was incrementally halted to allow recording of the strain, displacement and deflection. The specimens were loaded until ultimate failure occurred. The compression test data collected was imported into a Matlab computer routine to display the load-vs-strain results.

#### **B. IMPACT TESTING**

A drop weight impact tower was designed and built at the Naval Postgraduate school to conduct the impact tests

for this and future studies. The impact tower, depicted in Figure 3, consists of a sliding impactor guided by four stainless steel guide rods and the associated structural support. Precision linear bearing pillow blocks are used for the sliding impactor/guide rod interface, and the resulting sliding friction between the impactor and guide rods is negligible. The mass of the impactor may easily be varied by the addition or removal of specially designed weights. All tests during this study were performed with an impactor weight of either 21.79 N (4.9 lb<sub>f</sub>) or 50.71 N (11.4 lb<sub>f</sub>). The drop heights varied from 1.27 cm (0.5 in.) to 94 cm (37 in.).

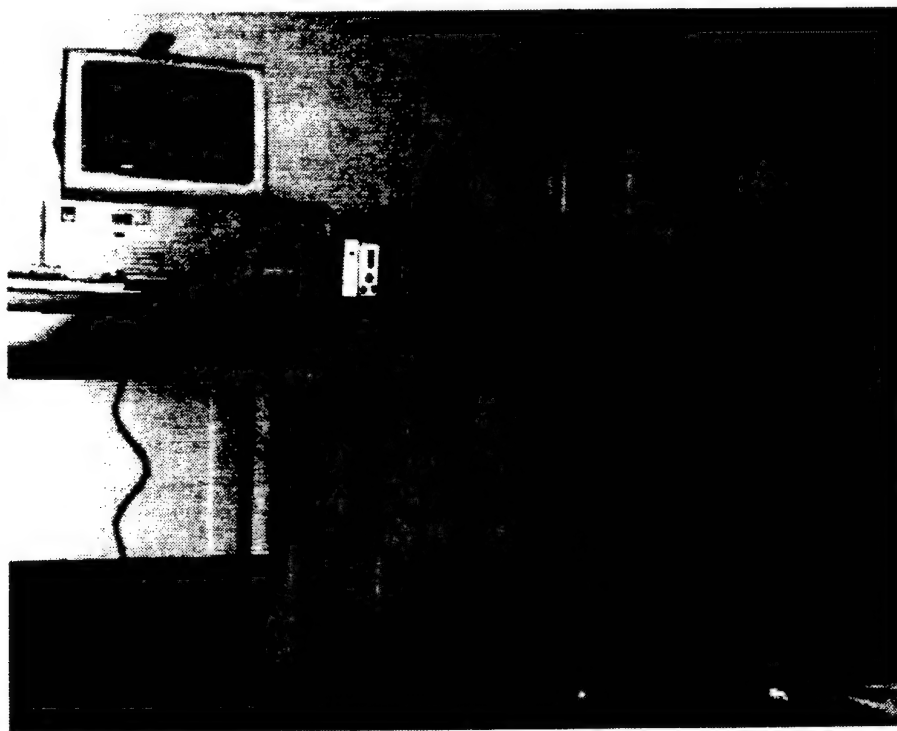


Figure 3. Impact Tower

A test sample fixture, solidly fastened to the impact tower structure, held the sample in the simply supported condition snugly. The fixture prevented lateral and vertical motion of the specimen-support contact points during impact. The sample was aligned on the support fixture to ensure the impactor head struck on the center of the sample. A thin strip of brass, 6.98x1.52x6.98 cm (2.75x 0.6x0.125 in.), was secured to the center of the impacted facesheet to spread the load over the width of the sample.

The actual impactor, attached to the sliding mass assembly, was a PCB Piezotronics force transducer Model 200A04 with a calibration range of 4448 N (0-1000 lbs.). The impact force transducer was powered by a PCB Piezotronics Model 482 line voltage power supply.

The test specimens were instrumented with five 1.27 cm (0.5 in.) Measurements Group, Inc. CEA-13-250UN-350 precision strain gages mounted longitudinally and centered on the width of the specimen. Two strain gages were placed at the quarter length points on the impacted facesheet and three strain gages were placed on the opposite side. Figure 4 depicts the strain gage placement. The strain gages were connected to an Ectron amplifier bridge Model E513-6A-M997.

The five strain gage outputs and the impact force transducer output were each assigned a channel on an analog to digital computer board in an IBM compatible P.C. with a



data acquisition program. The analog to digital converter and associated software limited the data acquisition sampling frequency to 4000 Hz. The strain gage and impact force transducer voltages were read and stored by the computer data acquisition system. The data was then imported into a Matlab routine for calculating the impact force and resulting microstrain using appropriate scaling factors previously determined for the specific impact load cell and strain gages used.

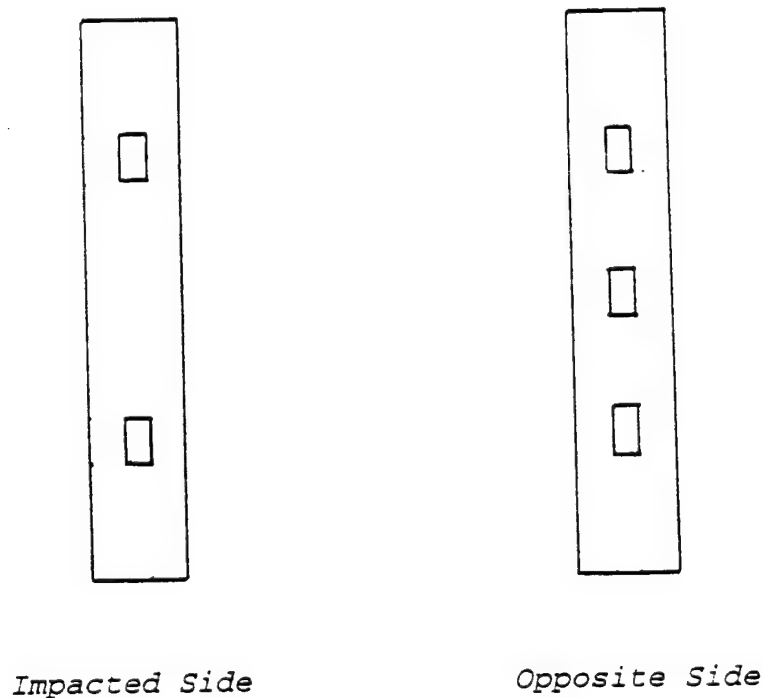


Figure 4. Strain Gage Placement

The energy of impact is varied for each impact test by varying the impact tower height. In performing a series of impact tests on any given sample the drop tower weight was kept fixed while the drop height was incrementally increased. For those samples not subjected to post impact compression tests, the tower height was incrementally increased until an indication of damage occurred. Any drop in load-vs-time or abrupt change in strain-vs-time was taken as an indication of damage.

As outlined by Crane and Juska [Ref. 1.], the force history information may be used to determine the acceleration, energy, velocity, and distance versus time information for the impact event. The force that is sensed by the impact load cell is the actual force applied to the composite test sample during the impact event (impactor mass times the acceleration of the impactor). The acceleration of the impactor is obtained from Newton's second law:

$$mg - F = ma \quad (1)$$

where the force on the composite,  $F$ , is the force read from the impact load cell and  $mg$  is the force due to gravity of the impactor. Equation (1) may be rearranged to solve for the acceleration,  $a$ , of the impactor during the impact event.

$$a = g - (F/m) \quad (2)$$

Substituting the weight of the impactor,  $w$ , into eq.(2) yields

$$a = (1 - (F/w))g \quad (3)$$

whereby the acceleration of the impactor is determined each time the impact force is measured. For this study, a sampling frequency of 4000 Hz was used, thus the force and strain data was sampled every 0.25 ms.

Equating the initial potential energy of the impactor before release with the kinetic energy at impact the initial velocity of the impactor at the instant of impact becomes

$$v = \sqrt{2gh} \quad (4)$$

The impactor velocity at any time during the impact event may be determined from the previous velocity and the average acceleration during the sampling time interval,  $t_i$  and  $t_{i-1}$ . The velocity is obtained by

$$v_i = v_{i-1} + ((a_i + a_{i-1}) / 2)dt \quad (5)$$

where  $dt$  is the time interval between sampling points. The displacement of the impactor during the impact event may be determined in a similar manner by

$$s_i = s_{i-1} + ((v_i + v_{i-1}) / 2)dt \quad (6)$$

The kinetic energy absorbed by the panel during the impact event, taken to be the loss in kinetic energy of the impactor, can then be determined by

$$T_i = T_{i-1} + \frac{1}{2}m(v_{i-1}^2 - v_i^2) \quad (7)$$

Furthermore, the work done on the specimen during the impact event may be determined from

$$W = \int f ds \quad (8)$$

and the momentum imparted to the specimen during the event may be determined from

$$M = \int f dt \quad (9)$$

Matlab routines were developed to calculate and plot Eqs. 2 through 7 versus time as well as to compute Eqs 8 and 9 using simple trapezoid rule integration.

#### **IV. EXPERIMENTAL RESULTS**

This section presents the results obtained from the individual experiments. The results are presented chronologically with discussion. After the pre-impact ultimate strength in compression was determined for each type of specimen, the impact tests were performed. After impact, several specimens were subjected to a post-impact compression test to determine the residual ultimate compression strength.

##### **A. PRE-IMPACT COMPRESSION TEST RESULTS**

The non-delaminated samples consisted of the symmetric sandwich composite with each sample having either a 0.3 cm (0.118 in.), 0.635 cm (0.25 in.) or 1.27 cm (0.5 in.) foam thickness. All delaminated samples had a 0.625 cm (0.25 in.) inch foam thickness and delamination lengths of 1.27 cm (0.5 in.), 2.54 cm (1.0 in.), 5.08 cm (2.0 in.), 10.16 cm (4.0 in.) inches or 15.24 cm (6.0 in.). The delamination was on one side only. Two identical compression tests were conducted on samples of the same type. The results of the two tests were very nearly identical, thereby confirming the test platform and procedures.

Figure 5 shows the general trend in the compression tests exhibited by all test samples. The test specimens displayed elastic behavior up to the critical point for

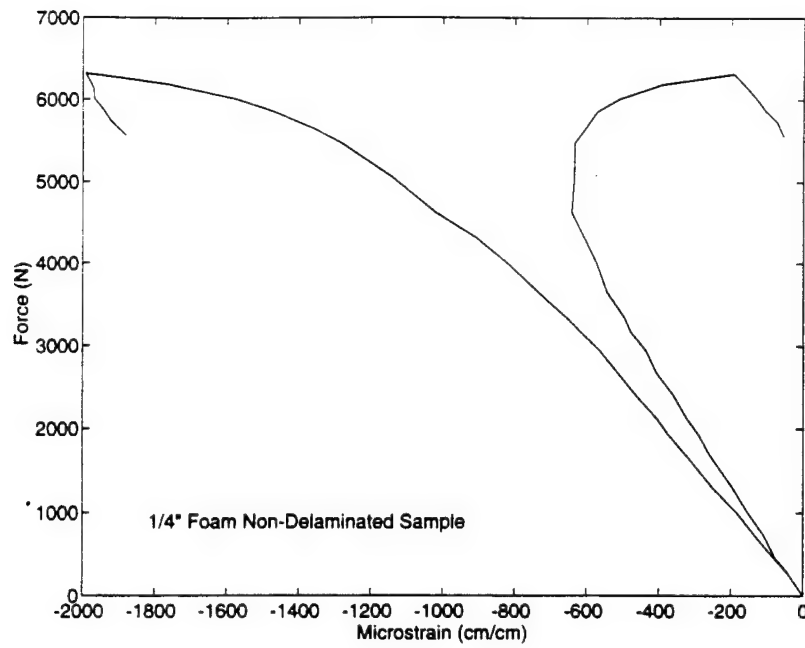


Figure 5. General Force-vs-Strain Trend in Compression

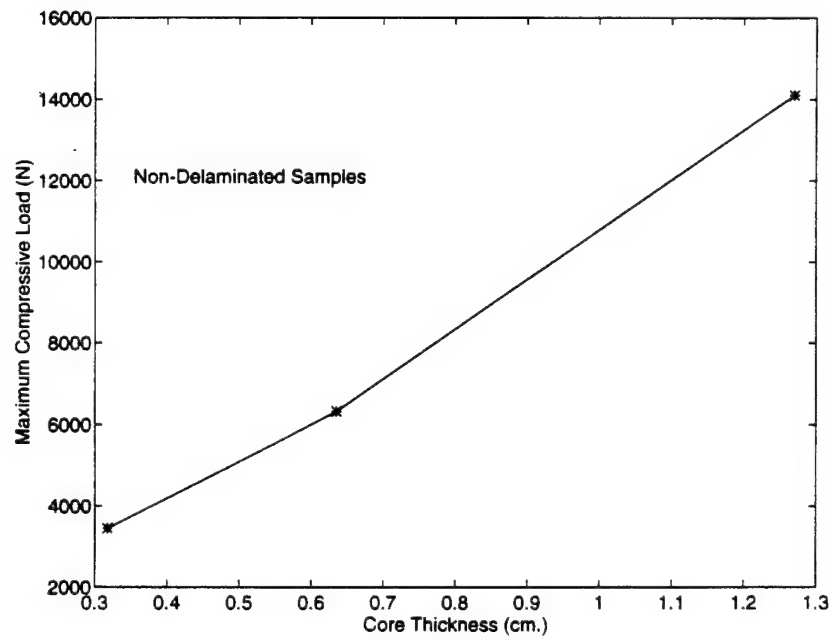


Figure 6. Maximum Compressive Load-vs-Core Thickness

buckling. Loading continued into the buckling regime until the ultimate load in compression was obtained and the sample began to shed the load quickly. Figure 6 shows the maximum compressive load-vs-core thickness for the non-delaminated samples. The maximum compressive load appears as an almost linear function of the core thickness. Figure 7 displays the maximum compressive load-vs-delamination length for the delaminated samples. There appears to be a threshold value of approximately 1112 N (250 lbf) where both the four and six inch samples failed. The maximum compressive load appears to an almost linear function of the delamination for the two, one and 1/2 inch delaminations.

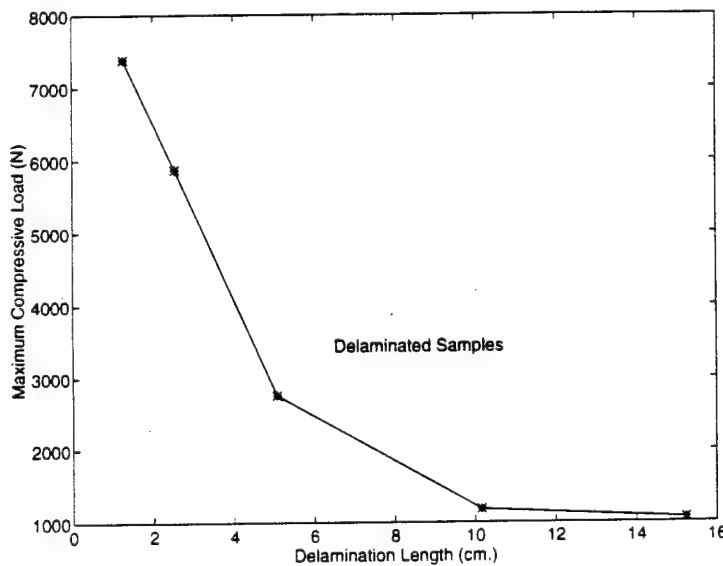


Figure 7. Maximum Compressive Load-vs-Delamination Length

None of the samples failed in the first mode of buckling as expected of a normal, isotropic material. Upon loading, the test samples would generally bend in the half-sine shape as expected of an isotropic material such as steel or aluminum, but with continued loading the sample would change from the half-sine shape to an 'S' shape. Figure 8 reveals the typical 'S' shape of a sample at failure. The delaminated samples showed no preference in bending toward or away from the side with delamination.



Figure 8. Typical 'S' Shape in Compression Failure



The failure mode of all samples, delaminated and non-delaminated, was failure by core shear. The core shear of the delaminated samples always originated at the edge of the delamination. The core shear of the non-delaminated samples generally originated at the quarter-length point on the sample. Note the maximum force in compression with one half inch delamination was actually greater than the maximum force of the sample without delamination: 7.69 kN (1730 lb.) versus 6.41 kN (1440 lb.).

#### **B. IMPACT TEST RESULTS**

Impact tests were conducted on all delaminated and non-delaminated specimen types. The original intent in this research was to begin impact testing on any given sample with a small energy of impact and to subsequently increase the energy of impact until an indication of damage was obtained. The damage would be manifested in a sudden drop of the impact force or a sudden change on the strain-vs-time graph of the impact event. The high stiffness of the test material renders it, along with most other sandwich composites, a brittle material. This brittle characteristic was reflected in the test samples absorbing all energy of impact elastically until the energy of impact was sufficient to cause catastrophic failure. No specimen,

delaminated or non-delaminated, displayed any visual sign of damage at any impact energy level below the level which caused catastrophic failure, and post-impact compression tests of samples which did not fail on impact resulted in an ultimate strength in compression equal to the pre-impact strength in compression  $\pm$  no more than 6 percent. Identical impact tests were conducted at least twice with repeating results. Compression tests were conducted on several 0.635 cm (0.25 in.) foam non-delaminated samples which had been subjected to catastrophic failure by impact, and the resulting ultimate load in compression was 311 N (70 lb<sub>f</sub>)  $\pm$  4%. This value, less than 1/3 the ultimate load in compression of even the six inch delaminated samples, can be considered the minimum compressive load carrying capability of the sandwich composite after catastrophic damage to the core and/or facesheet/core interface has occurred.

Figure 9 illustrates the typical impact force versus time, and Figure 10 depicts the typical strain versus time trend for the impact tests where failure did not occur. The relatively smooth trace of the resulting force and strain indicates no damage in terms of delamination occurred.

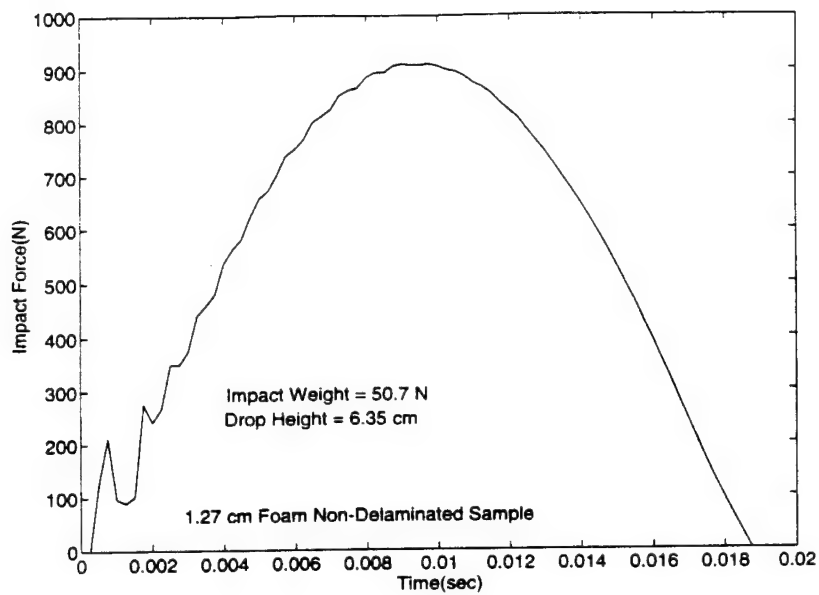


Figure 9. Force-vs-Time for Impact without Failure

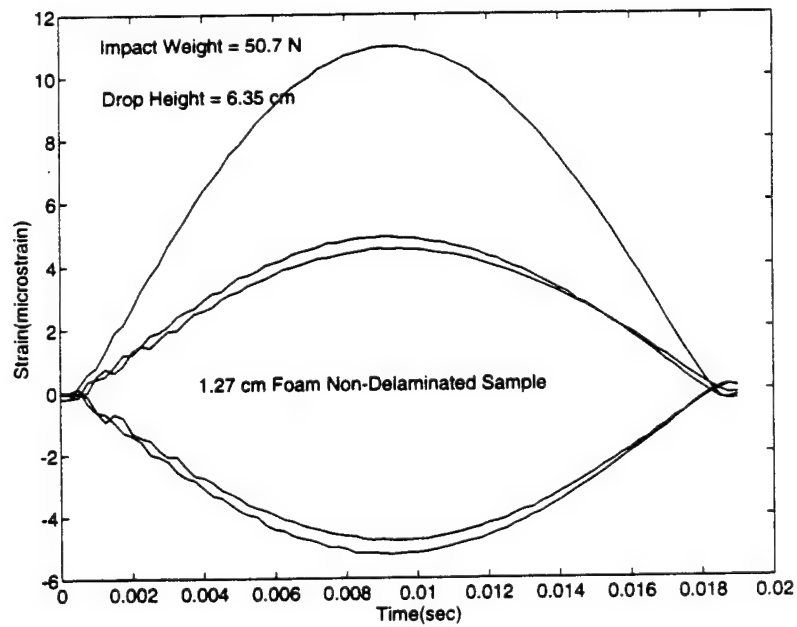


Figure 10. Strain-vs-Time for Impact Without Failure

Figures 11 and 12 reveal a typical failure event. Note the sudden changes in impact force and resulting strain. For a sample repeatedly impacted without failure, the maximum impact force and the maximum strain on impact would increase with increasing drop heights. On all tested samples, except the 15.24 cm (6.0 in.) delaminated samples, the absolute values of the strains at the quarter points on the impact facesheet were very nearly equal to the strains at the quarterpoints on the facesheet opposite the impact side. Tables I through III list the strain and force measurements obtained for the failure event of each sample type.

For the non-delaminated samples, the strain at the centerpoints of the samples was generally about two times the strain at the quarter points (Table I). This is just as expected from classical beam theory. The maximum strain at failure varied only from 9.5-12.1 microstrain even though the sample core thickness varied from 0.30-1.27 cm (0.118-0.5 in.). The failure mode of the non-delaminated samples was failure by core shear.

Impact on the non-delaminated side of the delaminated samples caused failure at much lower peak forces and strains for the 15.24 cm (6.0 in.), 10.16 cm (4.0 in.), and 5.08 cm (2.0 in.) delaminations (Table 2) than those of the

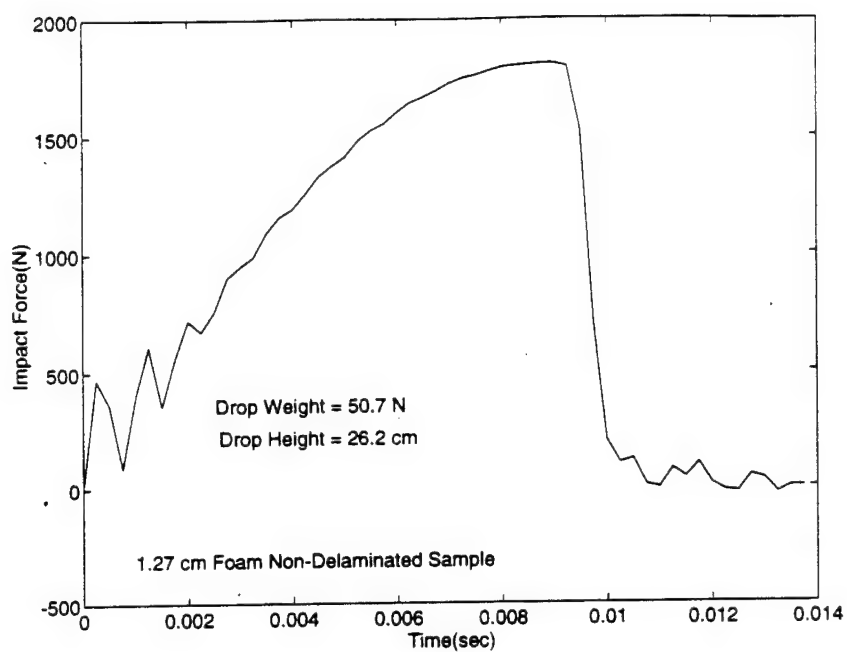


Figure 11. Force-vs-Time for Impact with Failure

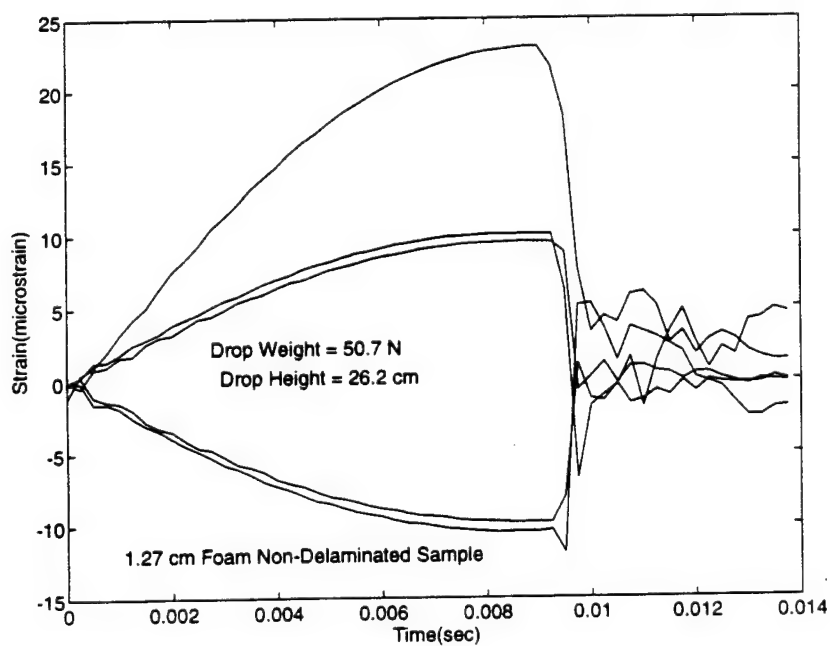


Figure 12. Strain-vs-Time for Impact with Failure

Foam Thickness (cm)	Drop Weight (N)	Drop Height (cm)	Max Force (N)	Max 1/4 Point Strain ( $\mu$ strain)	Max 1/2 Point Strain ( $\mu$ strain)
0.300	50.7	20.3	564.5	12.1	25.7
0.635	21.7	68.6	979.5	10.9	25.8
0.635	50.7	22.8	1128.0	11.1	27.2
1.270	50.7	26.2	1807.3	9.5	23.0

Table I. Non-Delaminated Sample Impact Response

Delam Length (cm)	Drop Weight (N)	Drop Height (cm)	Max Force (N)	Max 1/4 Point Strain ( $\mu$ strain)	Max 1/2 Point Strain ( $\mu$ strain)
15.24	21.7	2.5	161.5	3.4	9.8
10.16	21.7	5.1	277.6	2.8	10.5
5.08	21.7	20.3	613.8	8.0	17.7
2.54	21.7	66.0	943.0	11.2	27.2
1.27	21.7	83.8	1209.9	11.3	26.3

Table II. Delaminated Sample Response to Impact on Non-Delaminated Side

Delam Length (cm)	Drop Weight (N)	Drop Height (cm)	Max Force (N)	Max 1/4 Point Strain ( $\mu$ strain)	Max 1/2 Point Strain ( $\mu$ strain)
15.24	21.7	2.5	102.3	7.3	7.4
10.16	21.7	2.5	169.5	2.1	8.9
5.08	21.7	7.6	379.8	4.7	12.8
2.54	21.7	60.9	922.5	10.6	26.3
1.27	21.7	68.6	877.6	10.6	27.4

Table III. Delaminated Sample Response to Impact on Delaminated Side

non-delaminated 0.635 cm (0.25 in) foam samples. The mid-point strain is almost three times the quarterpoint strain for the 15.24 cm (6.0 in.) delamination, about four times the quarterpoint strain for the 10.16 cm (4.0 in.) delamination, and about two to two and a half times the quarterpoint strain for the 2.54 cm (1.0 in.) and the 1.27 cm (0.5 in.) delamination. The failure mode for the delaminated samples impacted on the non-delaminated side was failure by delamination spreading for the 10.16 cm (4.0 in.) and the 15.24 cm (6.0 in.) delamination samples and by core shear with attendant delamination for the other sizes

of delaminations. The one half inch delamination sample actually had a higher maximum force of impact than did the non-delaminated samples.

Comparing impact on the delaminated side with impact on the non-delaminated side, we note delaminated side impact case (Table III) force and strain trends much like those of the non-delaminated side impact. The maximum force of impact on the delaminated side was about 60 percent of the maximum force for impact on the non-delaminated side for the 15.24 cm (6.0 in.), 10.16 cm (4.0 in.) and 5.08 cm (2.0 in.) delamination samples. The maximum forces of the two 2.54 cm (1.0 in.) delaminated cases are nearly equal, but for the 1.27 cm (0.5 in.) delaminated cases the maximum force of the delaminated side impact case is only 72 percent of that of the non-delaminated side impact. The failure mode for delaminated side impact was always core shear originating at the edge of the delamination.

Before conducting the impact tests, it was intuitively expected that the duration of the impact event would increase for increasing drop heights for samples that do not fail. This was not the case. The impact duration for any given undamaged sample remained constant  $\pm 1$  ms as the impactor was dropped from increasing heights. For the non-



delaminated samples, the impact duration increased with decreasing core thickness. Table IV lists the duration of

<b>Non-Delam Samples</b>		
Foam Thickness (cm)	Drop Weight (N)	Impact Duration (ms)
0.300	50.7	52
0.635	21.7	20
0.635	50.7	31
1.270	50.7	18
<b>Impact Non-Delam Side</b>		
Delam Length (cm)	Weight (N)	Impact Duration (ms)
15.24	21.7	33
10.16	21.7	23
5.08	21.7	19
2.54	21.7	21
1.27	21.7	18
<b>Impact Delam Side</b>		
Delam Length (cm)	Weight (N)	Impact Duration (ms)
15.24	21.7	43
10.16	21.7	25
5.08	21.7	20
2.54	21.7	20
1.27	21.7	18

TABLE IV: Impact Time of Duration

various impact events. The varying impact time for the different foam thicknesses is deemed to be a function of the global stiffness of the impact specimen. The thicker cores, having a larger cross-sectional area, had a higher global stiffness value and released the strain energy of bending resulting from the impact faster than the samples

with the thinner cores. The duration of impact increased with increasing drop weight until failure. For the delaminated samples, the 15.24 cm (6 in.) delaminated sample impacted on the non-delaminated side had a duration 23% shorter than the duration of the sample impacted on the delaminated side. For other delamination lengths the duration for each impact side varied by 8% or less. The duration of impact increased as the length of delamination increased. This is in concurrence with the above discussion as the increased length of delamination causes a decrease in the stiffness of the material.

The force histories for each impact event were used to calculate the kinetic energy imparted to the sample, the work done on the sample,  $\int f ds$ , by the impactor and the momentum imparted,  $\int f dt$ , to the sample. Figures 13-17 are the typical force, velocity, displacement, and kinetic energy-vs-time and the typical force-vs-displacement curves for the impact without failure. These particular graphs are the result of 50.7 N (11.4 lb<sub>f</sub>) drop weight from 6.35 cm (2.5 in.) on a non-delaminated 1.27 cm (0.5 in.) foam sample. Figures 18-22 show the same quantities for the same sample for the failure event which occurred at a drop height of 26.2 cm (10.3 in.). These graphs are typical of

failure events for all sample types. Table V lists the various energy quantities obtained for each failure event.

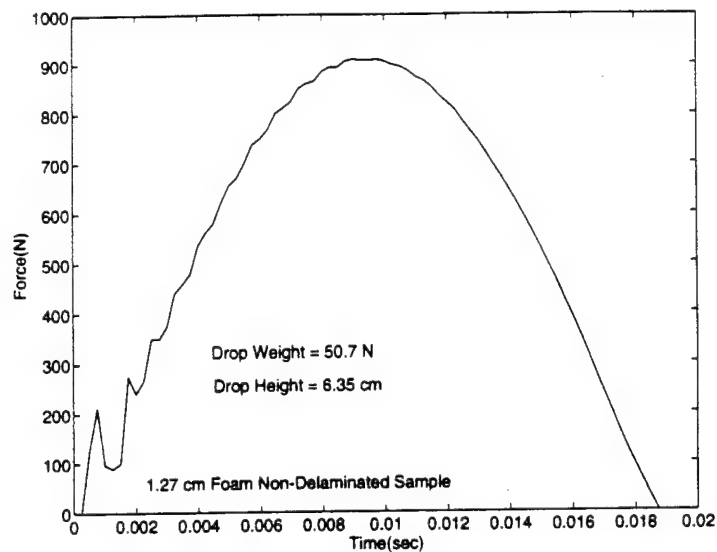


Figure 13. Force-vs-Time for Impact Event

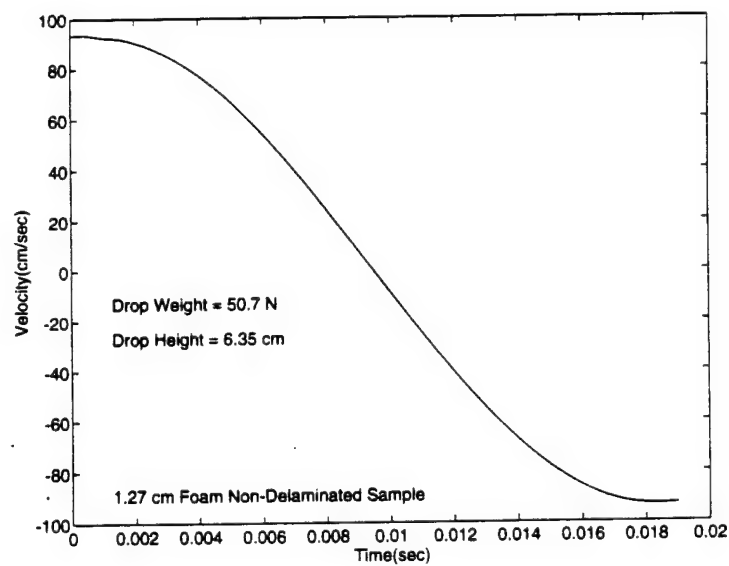


Figure 14. Velocity-vs-Time for Impact Event

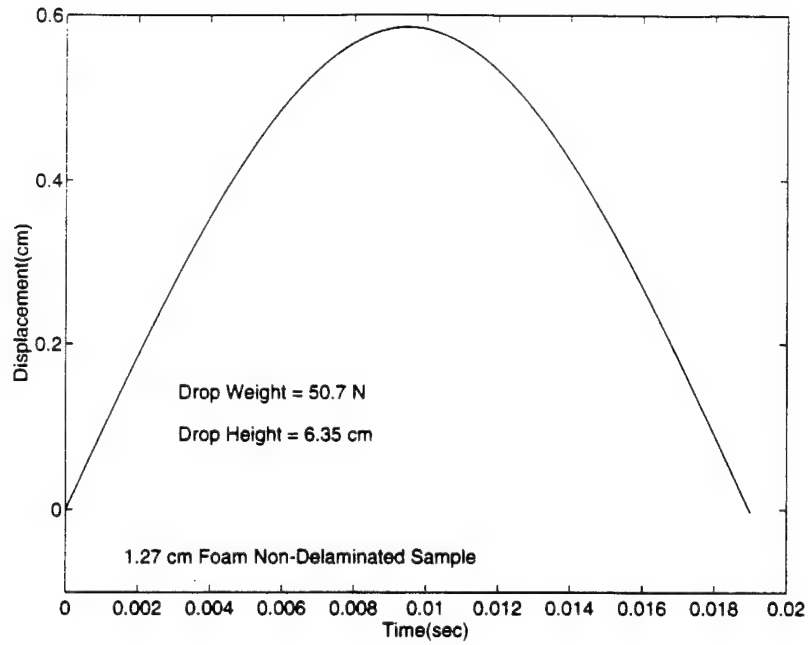


Figure 15. Displacement-vs-Time for Impact Event

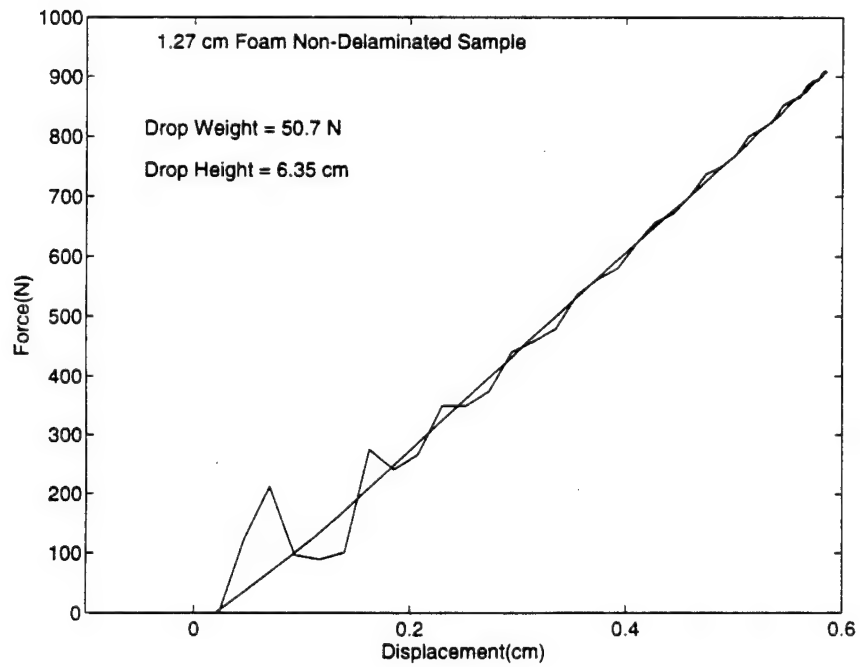


Figure 16. Force-vs-Displacement for Impact Event

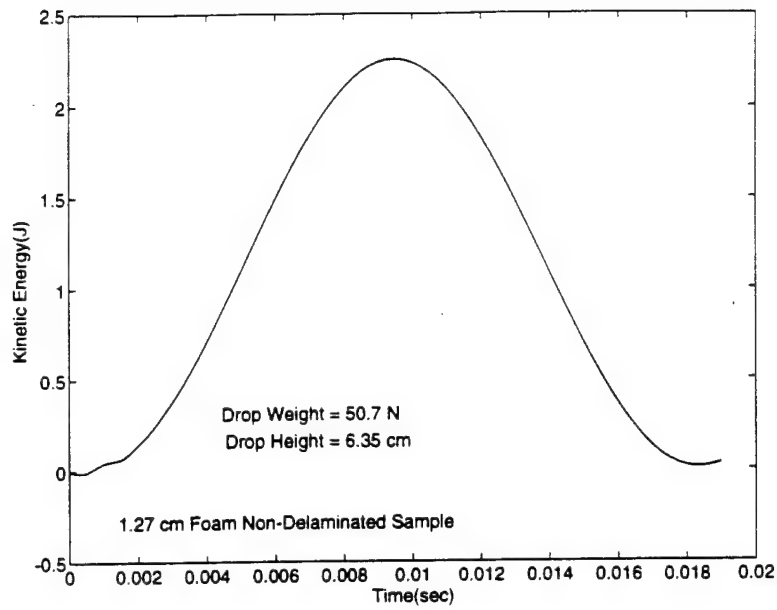


Figure 17. Kinetic Energy Imparted-vs-Time for Impact Event

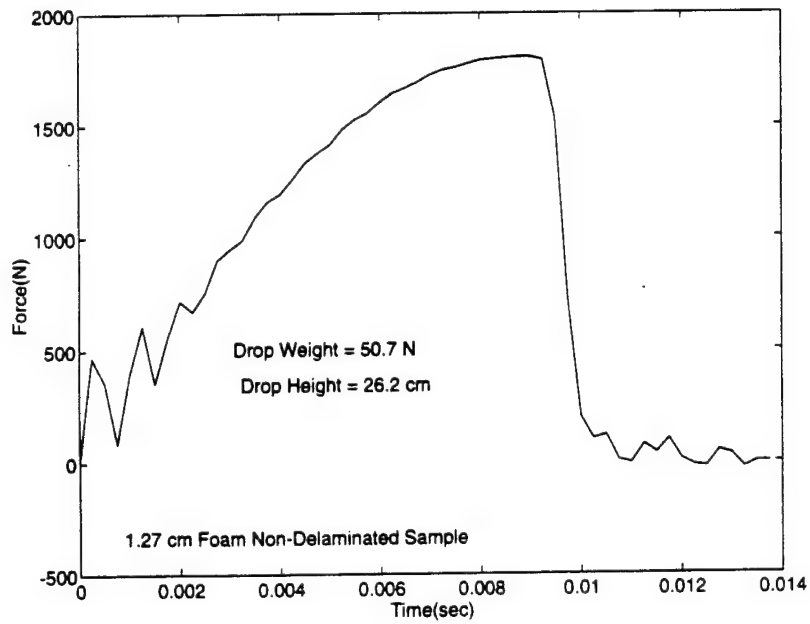


Figure 18. Force-vs-Time for Impact Failure

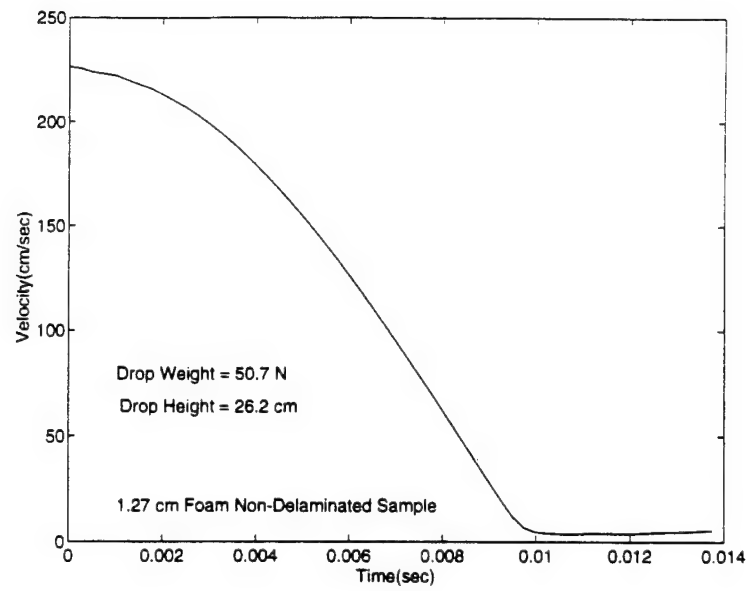


Figure 19. Velocity-vs-Time for Impact Failure

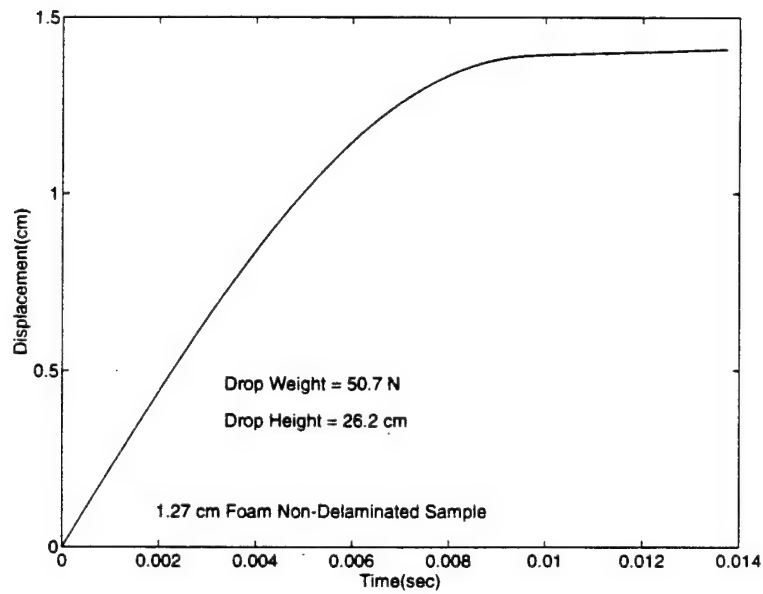


Figure 20. Displacement-vs-Time for Impact Failure

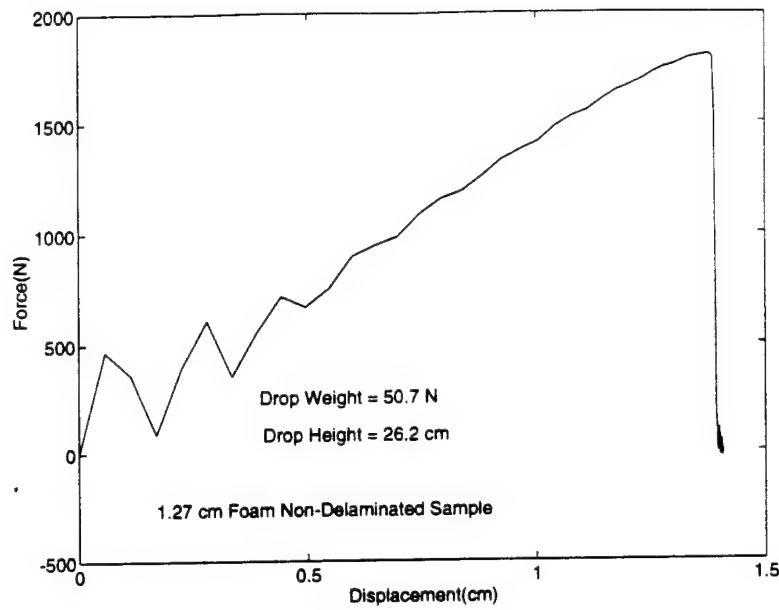


Figure 21. Force-vs-Displacement for Impact Failure

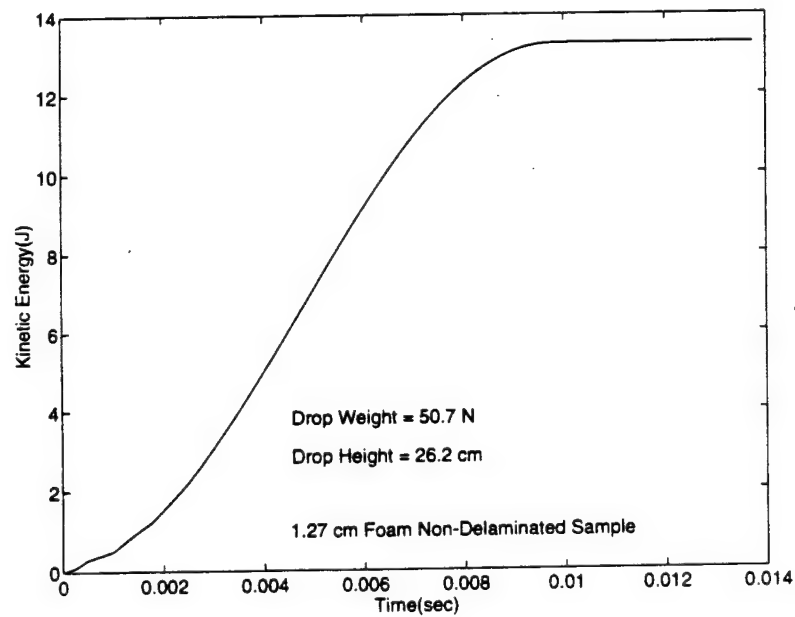


Figure 22. Kinetic Energy Imparted-vs-Time for Impact Failure

<b>Non-Delam Samples</b>				
Foam Thickness (cm)	Weight/Height (N/cm)	Momentum (N-m)	Work (N-m)	K.E (N-m)
0.300	50.71/20.3	1.5	14.8	12.5
0.635	21.7/68.6	1.4	12.5	11.4
0.635	50.7/22.9	2.9	12.5	11.3
1.270	50.7/26.2	3.8	12.5	13.2
<b>Impact Non-Delam Side</b>				
Delam Length (cm)	Weight/Height (N/cm)	Momentum (N-m)	Work (N-m)	K.E. (N-m)
15.24	21.7/2.5	0.7	0.4	0.3
10.16	21.7/5.1	0.4	0.9	0.8
5.08	21.7/20.3	0.8	4.2	3.5
2.54	21.7/66.0	1.8	15.1	13.0
1.27	21.7/83.8	2.0	19.4	16.5
<b>Impact Delam Side</b>				
Delam Length (cm)	Weight/Height (N/cm)	Momentum (N-m)	Work (N-m)	K.E. (N-m)
15.24	21.7/2.5	0.9	0.8	0.5
10.16	21.7/2.5	0.7	1.2	0.5
5.08	21.7/7.6	0.7	1.8	1.5
2.54	21.7/61.0	1.5	10.4	11.7
1.27	21.7/68.6	1.2	11.4	10.4

TABLE V: Impact Energies of Failure

Observing Figures 13-17 for the impact event without failure, we are able to verify our velocity, distance and energy calculations are qualitatively correct. Note that the velocity of the impact assembly leaves the specimen with less than the impact velocity. Note also that the displacement at impact returns to zero, and that no



hysteresis exists on the Force-vs-Displacement curve. As the drop height is increased and damage occurs, the Force-vs-Displacement hysteresis loop becomes more pronounced. The graphs of all impact failure events are included in the appendix.

To observe failure differences with varying drop weight, height and velocity, the 0.635 cm (0.25 in) non-delaminated samples were impacted with 50.71 N (11.4 lb<sub>f</sub>) and 21.79 N (4.9 lb<sub>f</sub>) at heights resulting in the two tests having the same potential energy at the impactor's release. The lower-weight impact test required a higher initial potential energy to induce failure than did the test with the heavier drop weight. The work done on the samples and the kinetic energy imparted to the samples from the failure impact varied by less than one percent. The maximum force of impact varied by twelve percent, and the momentum imparted to the samples varied by over 100 percent. This indicates that the kinetic energy imparted and work done on the sample, vice the force of impact, momentum imparted or initial potential energy are the indicators which need to be observed in studying the failure mechanisms involved in impact failure.

The work done and kinetic energy imparted to the delaminated samples were small in magnitude for the six,

four and two inch delamination lengths as compared to the non-delaminated samples. The work done and kinetic energy imparted to the 2.54 cm (1.0 in.) and the 1.27 cm (0.5 in.) delaminated sample impacted on the non-delaminated side was greater than that of the non-delaminated samples. This, just as the higher compressive load at failure of the 1.27 cm (0.5 in) delaminated sample, goes against all reasoning, but the same phenomenon has been reported in experiments for delaminated composites [Ref. 7].

Overall, the trend observed throughout the impact testing was just as expected. The non-delaminated samples generally withstood greater impact energies, and the resulting forces and strains, before failure than did the delaminated samples. As the core material carries the major portion of the shear stresses that develop during the impact loading, any discontinuity or abrupt irregularity, such as a large scale delamination area, becomes a crack initiation site in the foam material, and failure by core shear results. Realizing the most prevalent observed damage of a foam core sandwich composite subject to low-energy impact occurs at the impacted facesheet/core interface, we expected the impact on the delaminated side to result in failure energies, and the resulting forces and

strains, less than those for impact on the non-delaminated side. Such is the trend observed.

Although enhanced composite fracture toughness and higher compressive strength to failure for composites with intermittent laminar debonding have been reported by several groups, this testing was not expected to result in greater failure energies (kinetic energy imparted) of the delaminated samples as found in the 1.27 cm (0.5 in.) and 2.54 cm (1 in.) delaminated samples impacted on the non-delaminated side. The reports of higher toughness and strength were from tests conducted on monolithic laminate composites. The 1.27 cm (0.05 in.) delaminated sample withstood a greater compressive force to failure than did the non-delaminated sample: 7.69 kN (1730 lb.) versus 6.41 kN (1440 lb.). This is believed to result from in the crack blunting process explained earlier. As the specimen was axially loaded beyond the critical load for buckling, the characteristic 'S' shape would invariably result. The 'S' shape resulted in high bending stresses in the faceplates, and the small delamination length effectively arrested the crack from propagating from the faceplates through the core. With delamination lengths greater than 1.27 cm (0.5 in), the loss of shear carrying capability becomes dominant, and the specimen fails by core shear at the

geometric irregularity existing at the edge of the delamination. The crack blunting theory probably cannot be imposed to explain the higher impact fracture energy of the 1.27 cm (0.5 in.) and 2.54 cm (1.0 in.) delaminated samples impacted on the non-delaminated side. Further testing using X-ray, C-scan, microscopy or other damage detection technique must be performed to ascertain the damage propagation mechanisms in those cases.

## V. CONCLUSIONS

It has been shown that the response of symmetric sandwich composites subjected to impact and/or compression loading is complex. The results are often opposite those expected, and much testing is required to collect sufficient data to understand exactly which test parameters are driving the results. More tests are still required, in conjunction with damage detection techniques, to ascertain the exact mechanisms involved in the damage of the symmetric sandwich composite.

The key findings of this research are:

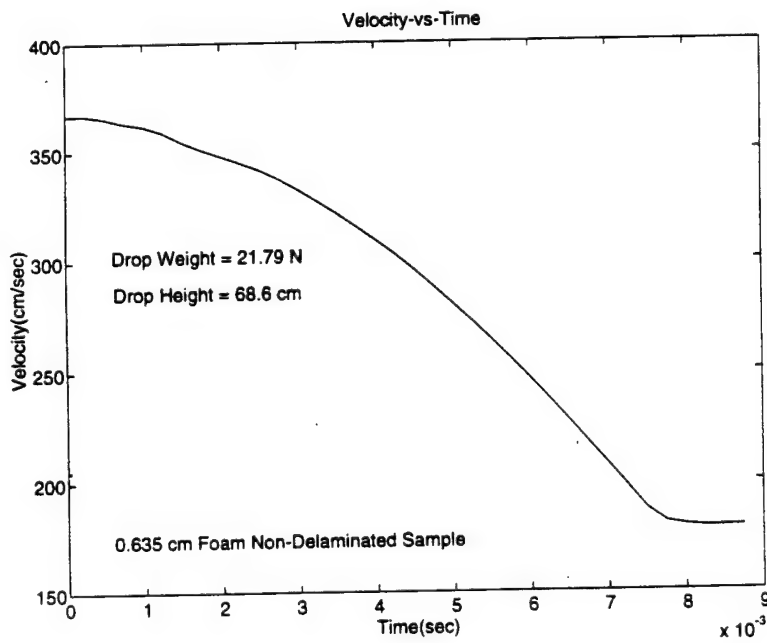
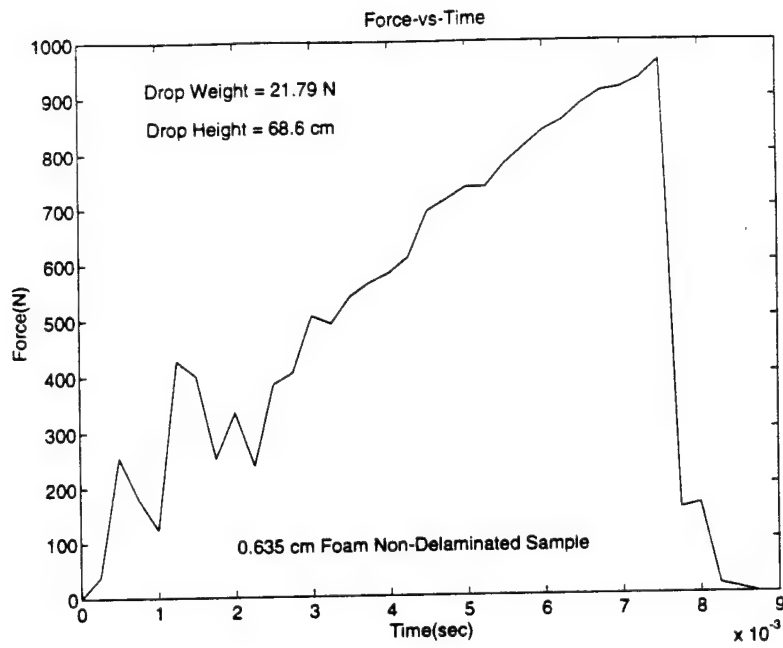
- The drop weight impact tower designed and built for this and future studies performed well, and, while used in conjunction with the data acquisition system, accurate force histories were obtained.
- The force history information may be used to develop equations for the kinetic energy and momentum imparted to the specimen and the work done on the specimen. The kinetic energy imparted to and work done on the specimen are the more prominent factors in failure as opposed to the force of impact, momentum imparted or initial potential energy of the impactor.
- As the core thickness was increased on the non delaminated samples, the maximum force of impact at failure increased, but the kinetic energy transferred remained relatively constant.
- The maximum force and kinetic energy absorbed in impact were much less for the 15.24 cm (6.0 in.), 10.16 cm (4.0 in.) and 5.08 cm (2.0 in) delaminated samples than for the non-delaminated samples. The values were almost equal for the 2.54 cm (1.0 in.) delamination case, but the 1.27 cm (0.5 in.)

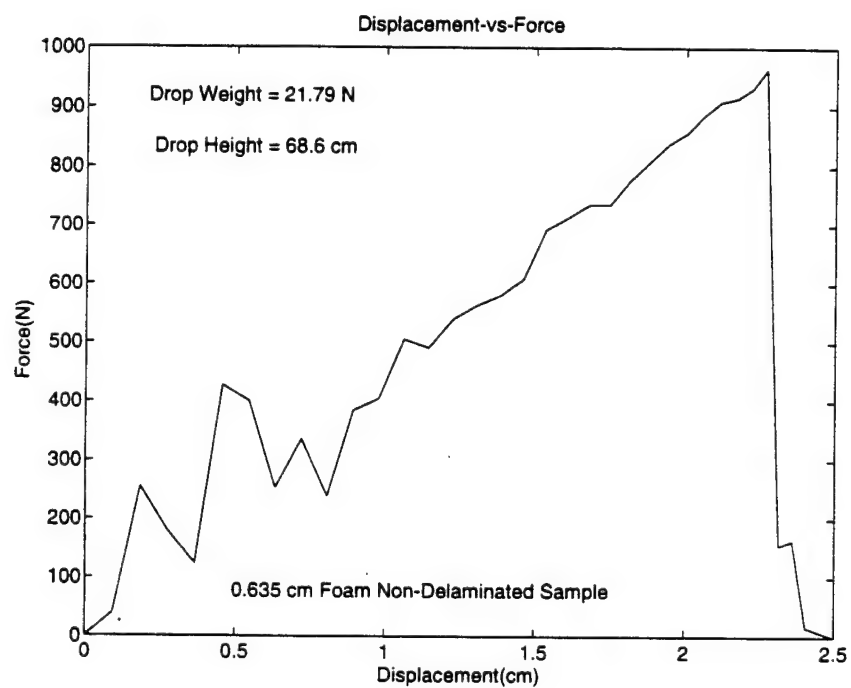
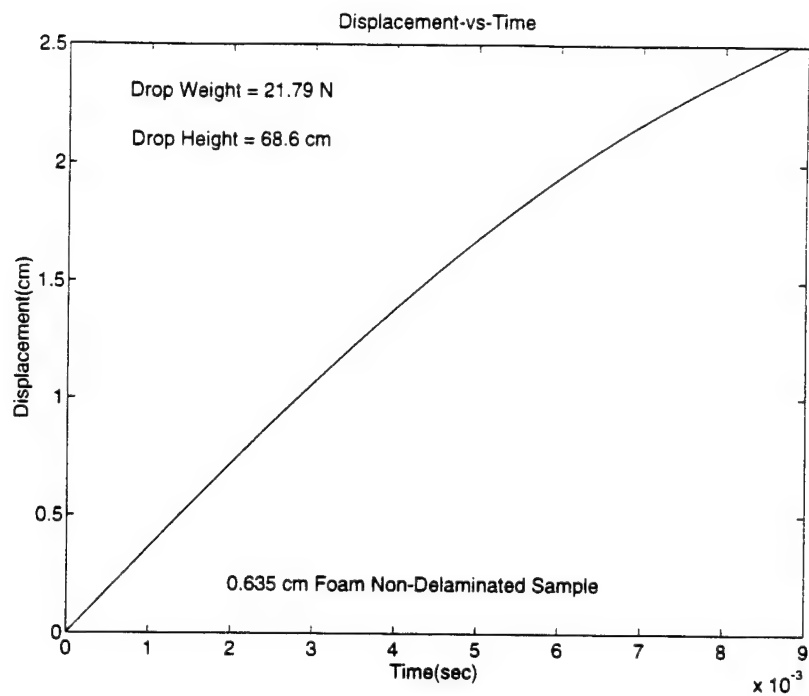
delaminated sample impacted on the non-delaminated side absorbed more kinetic energy to failure than did the non-delaminated samples. Furthermore, the 1.27 cm (0.5 in.) delaminated samples withstood a greater compressive load to failure than did the non-delaminated sample. For the delaminated samples, failure occurred at lower energies with impact on the delaminated side than with impact on the non-delaminated side.

- No specimen displayed any visual sign of damage, including sharp drops in the impact force-vs-time or strain-vs-time plots, until impacted with an energy level which resulted in catastrophic failure.
- Virtually all impact tests resulted in failure by core shear, but the 15.24 cm (6.0 in.) and the 10.16 cm (4.0 in.) delaminated samples impacted on the non-delaminated side failed by delamination growth. The compressive strength after failure by impact was negligible for all samples.

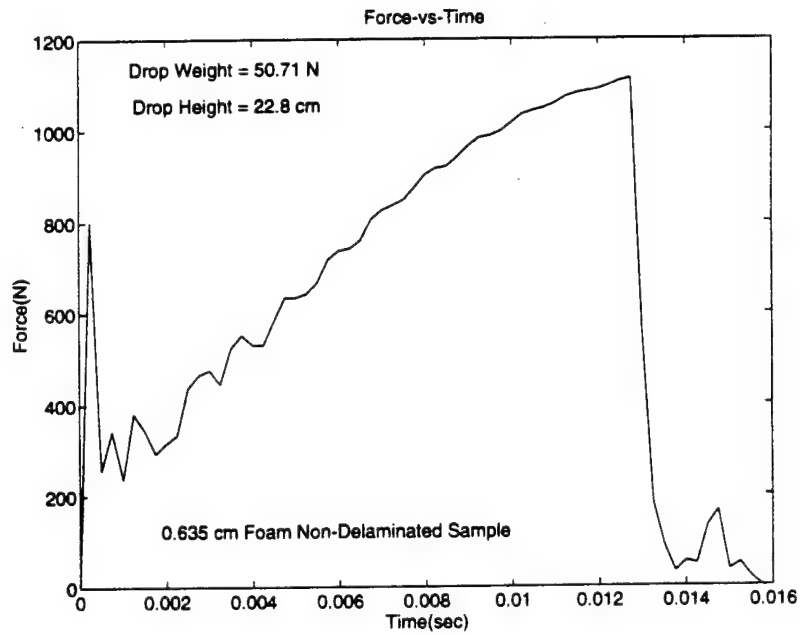
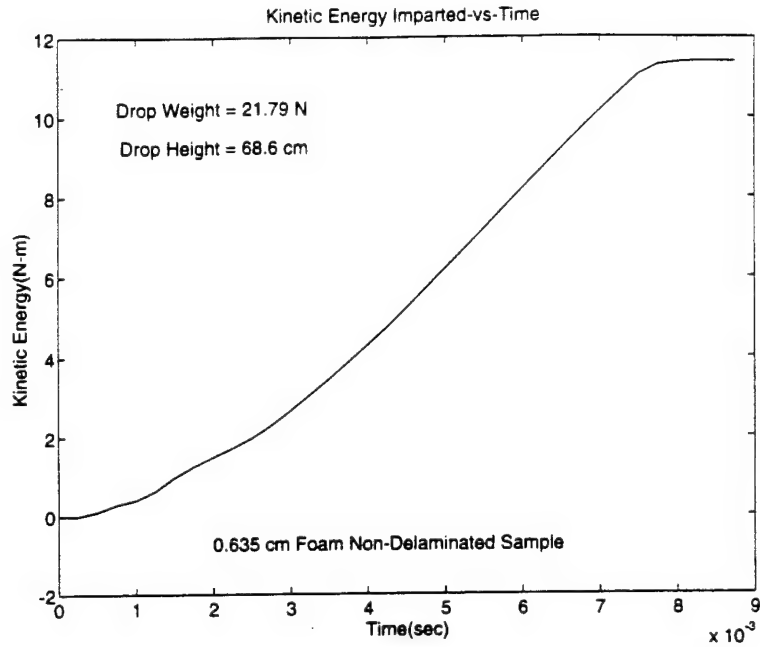
Continued testing with damage inspection must be performed to investigate the damage propagation. With a better understanding of the damage propagation mechanisms, we will gain better insight to the difference in toughness found in the non-delaminated as opposed to the delaminated samples.

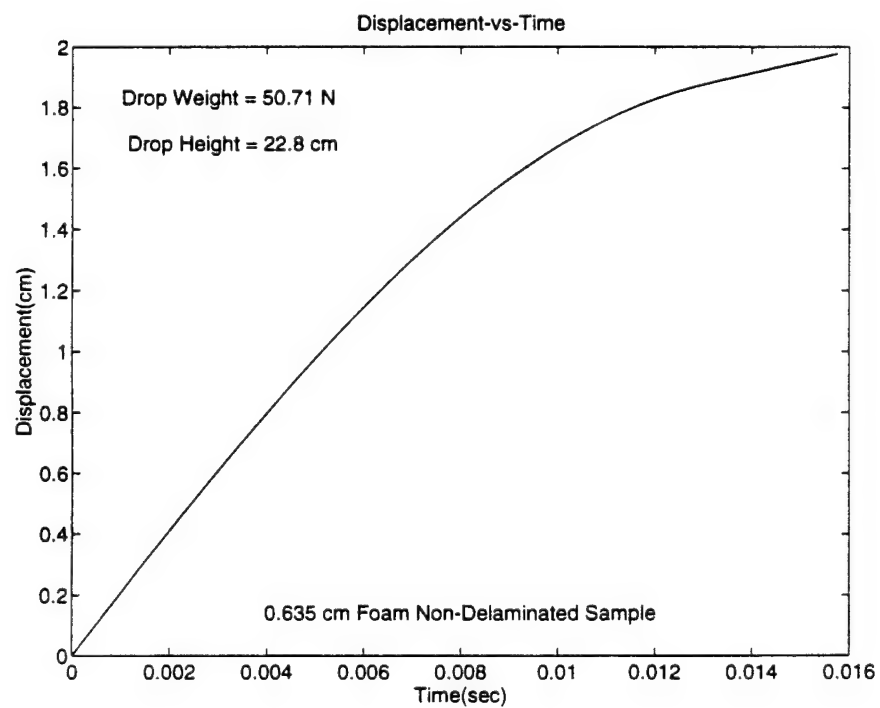
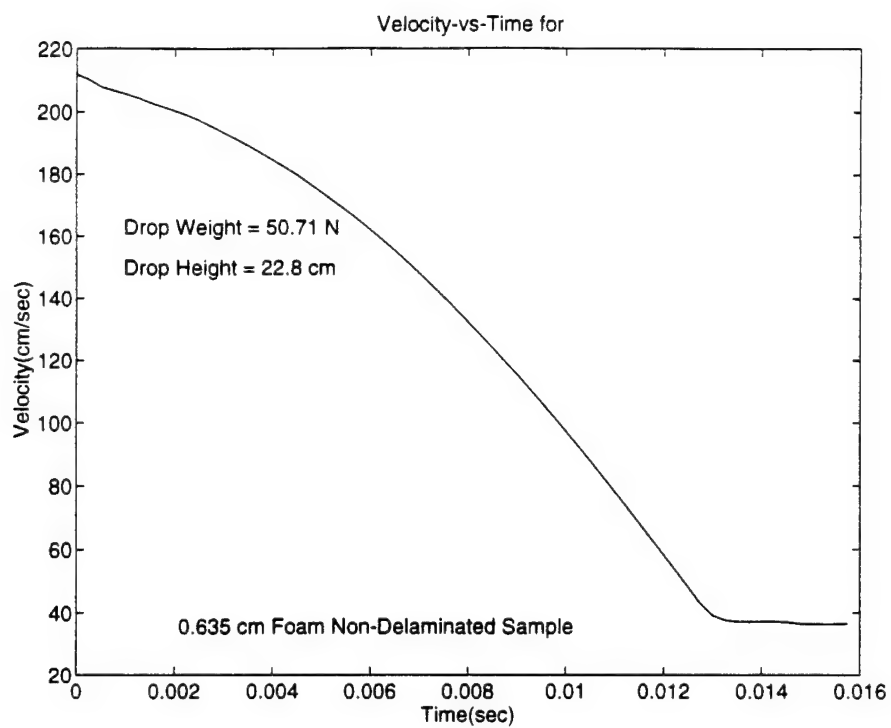
## APPENDIX

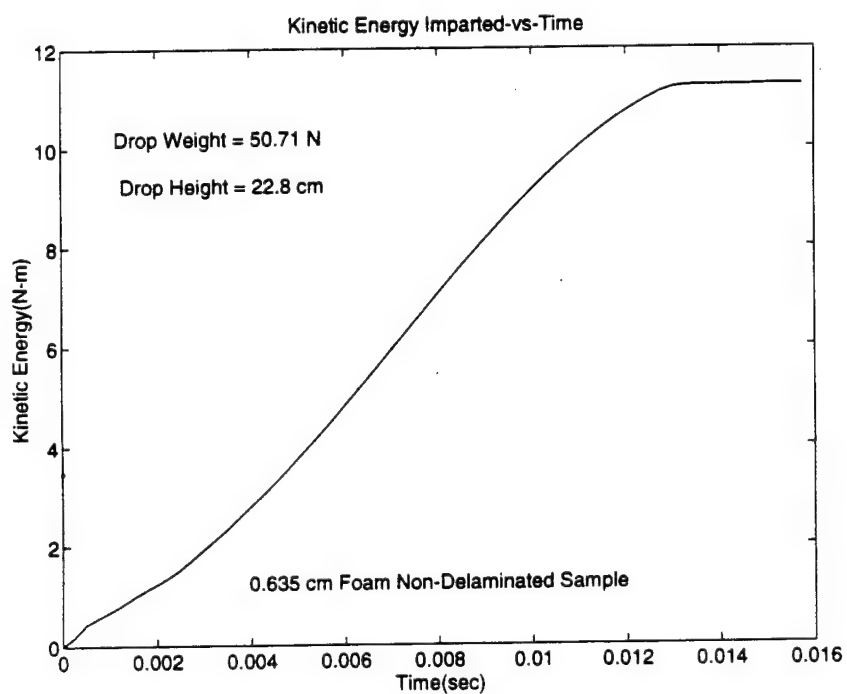
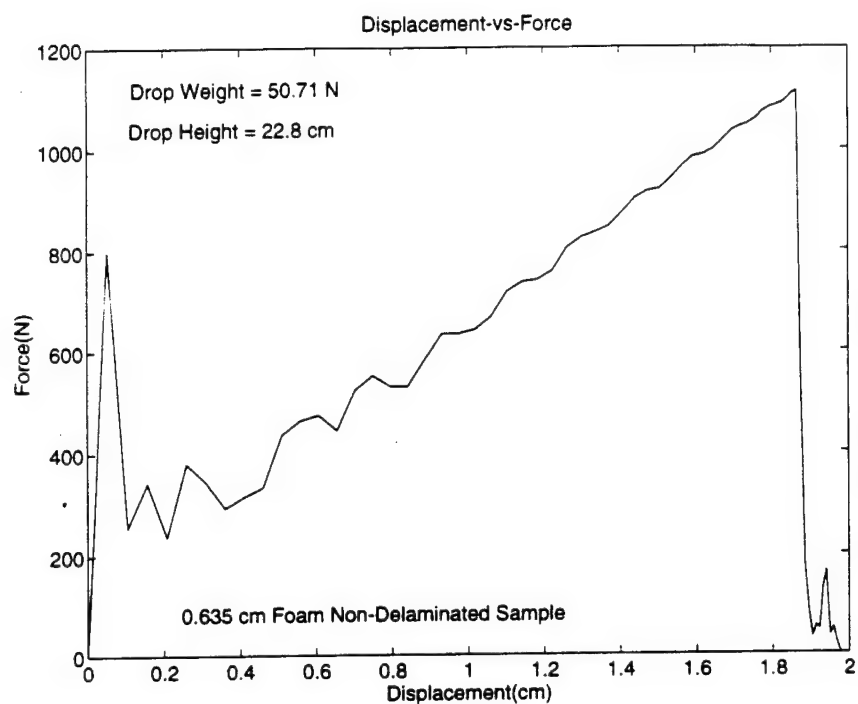


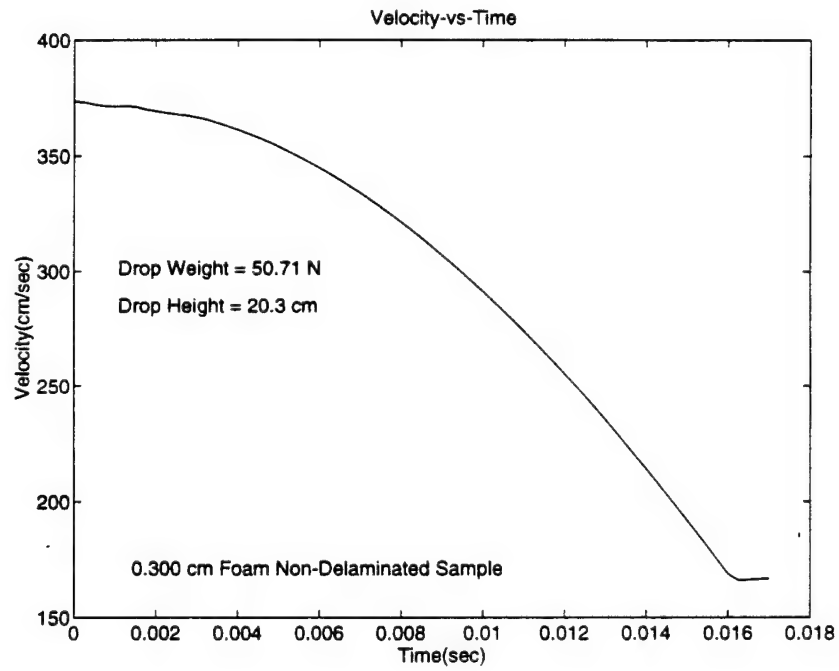
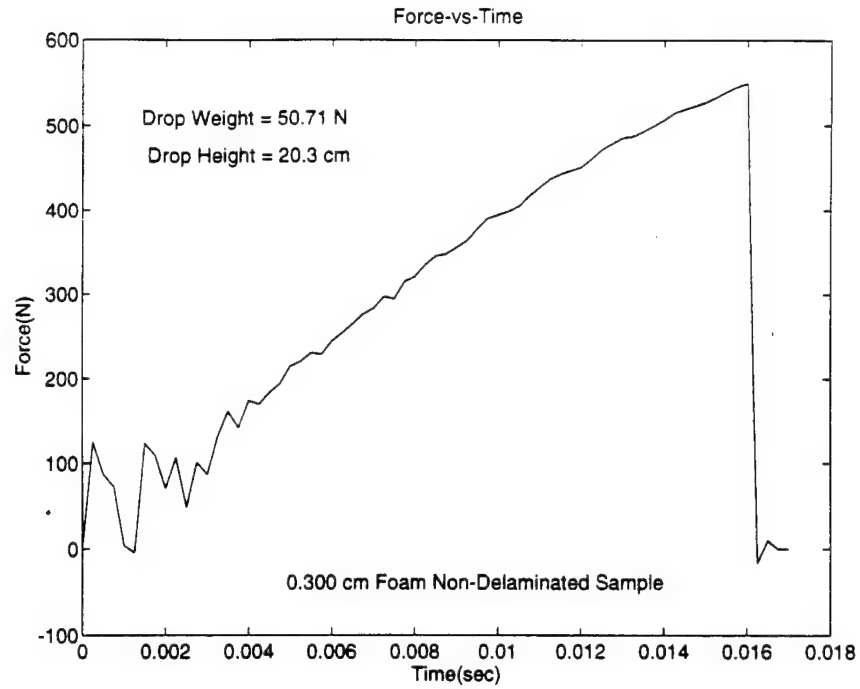


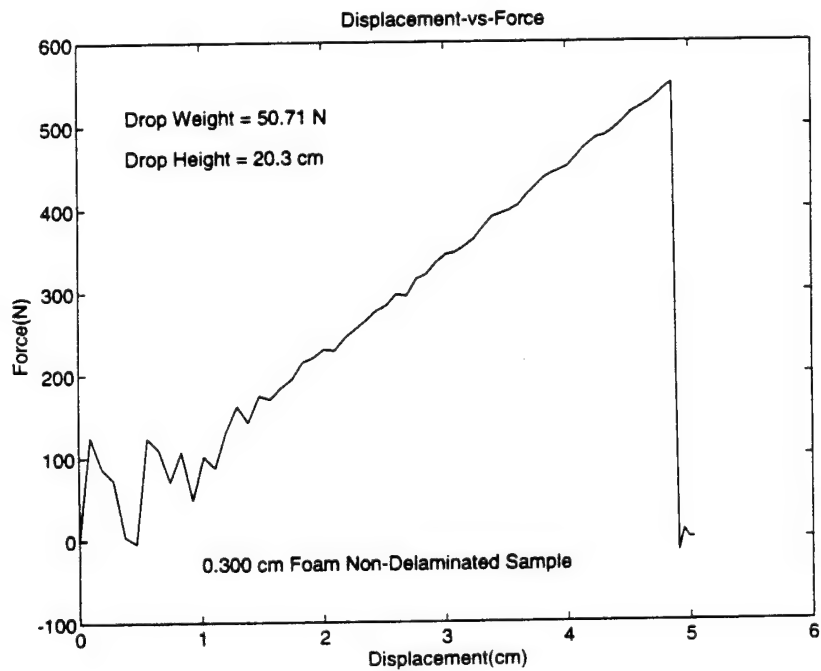
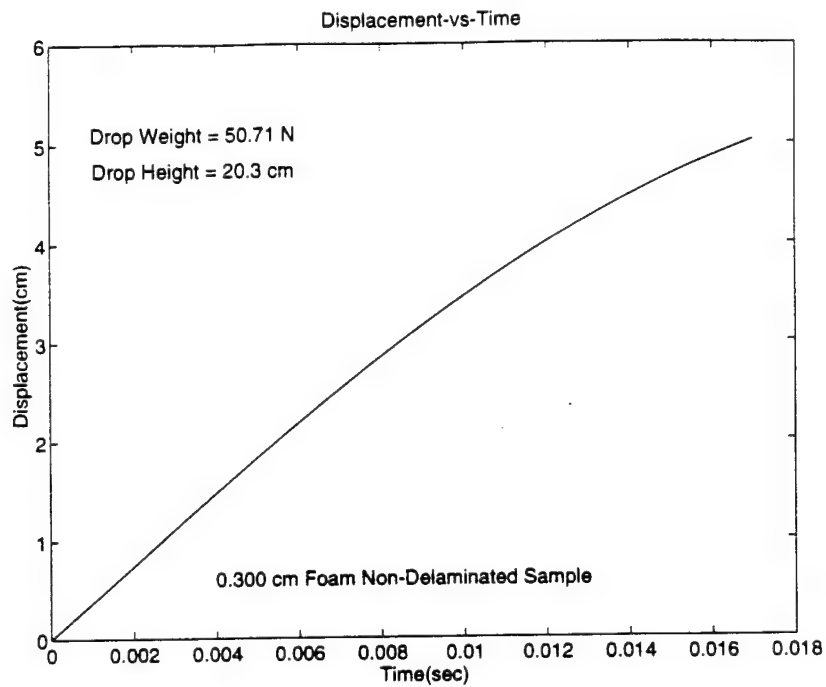


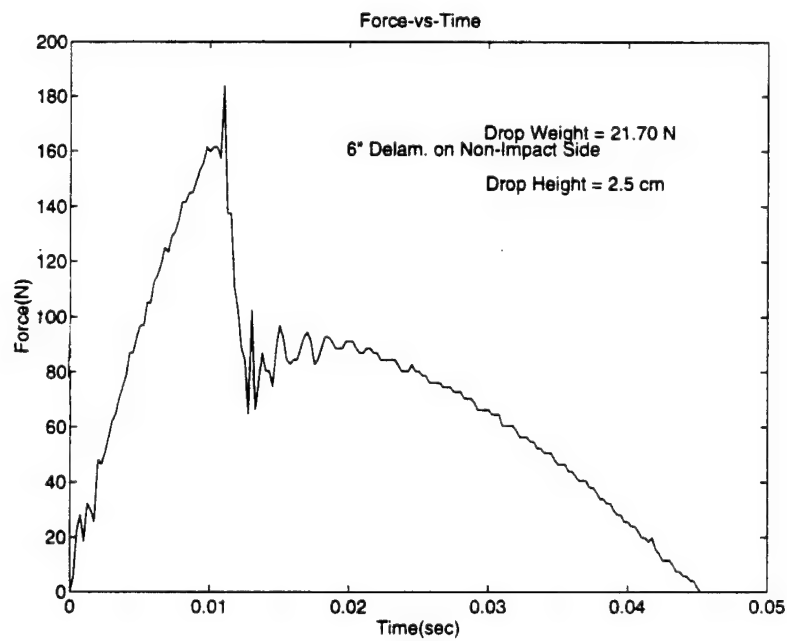
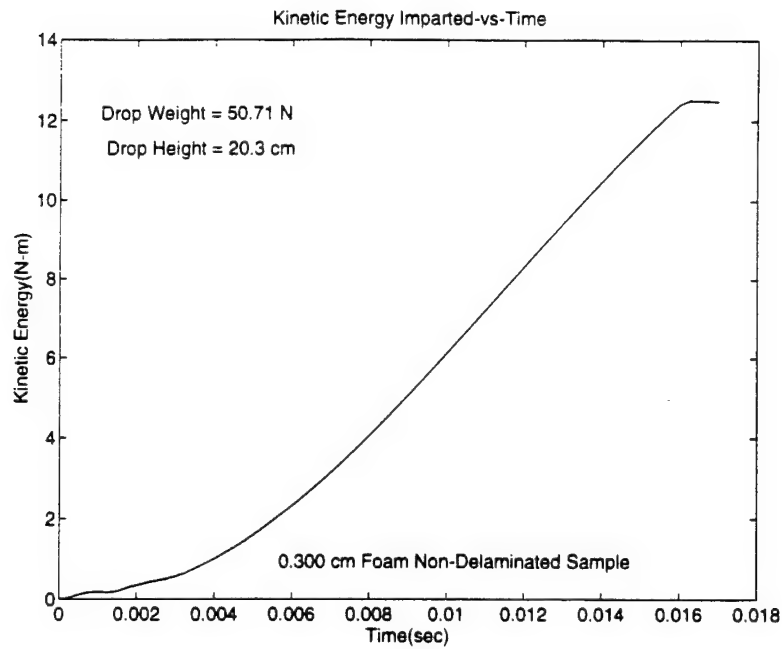


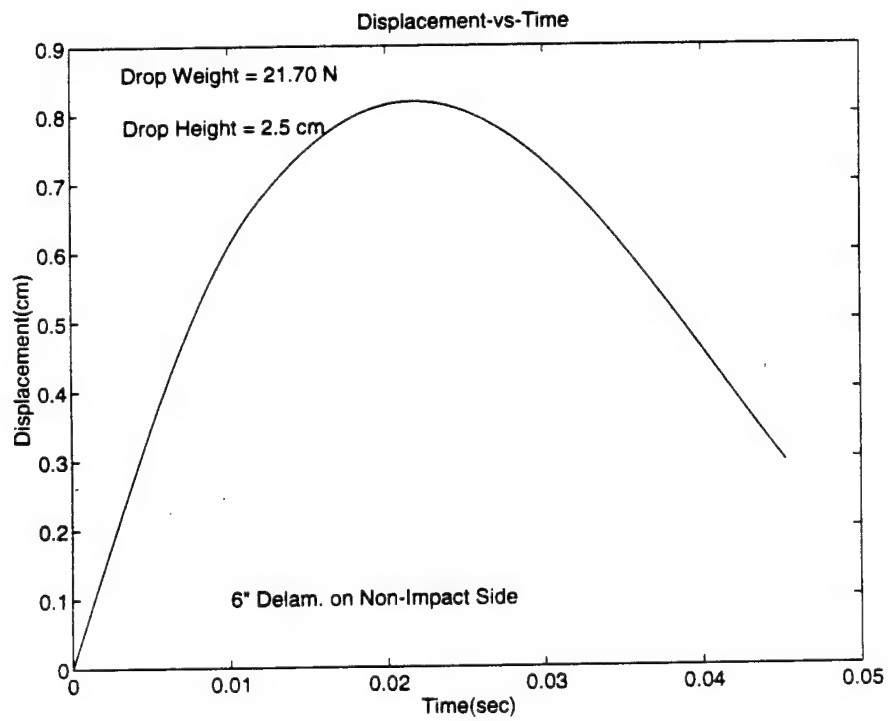
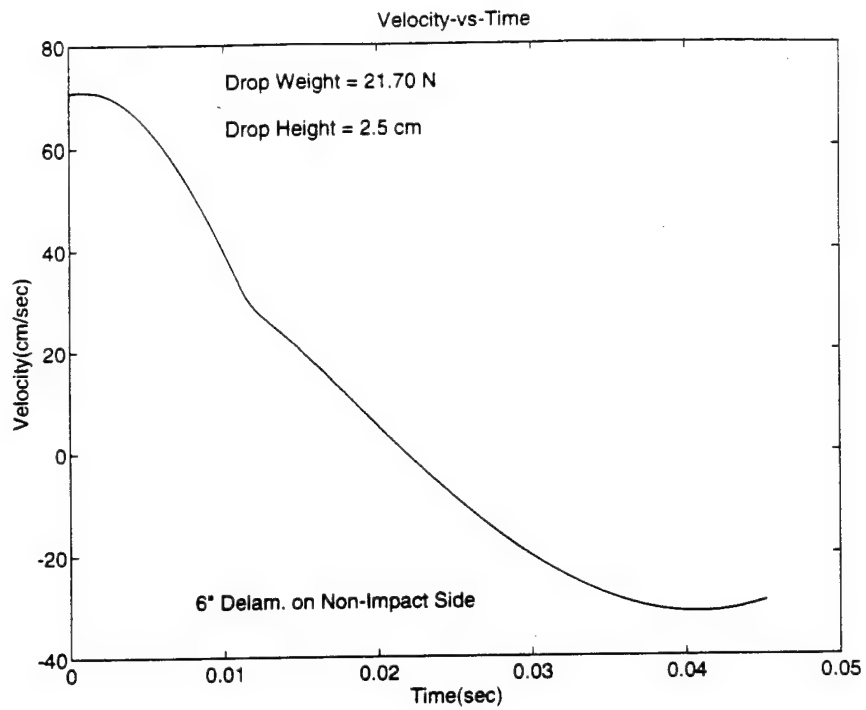


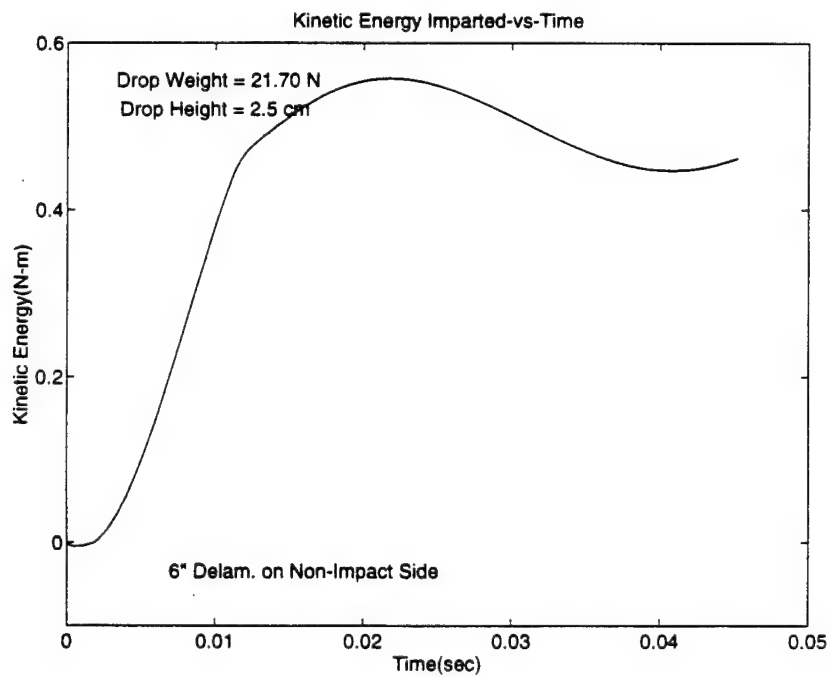
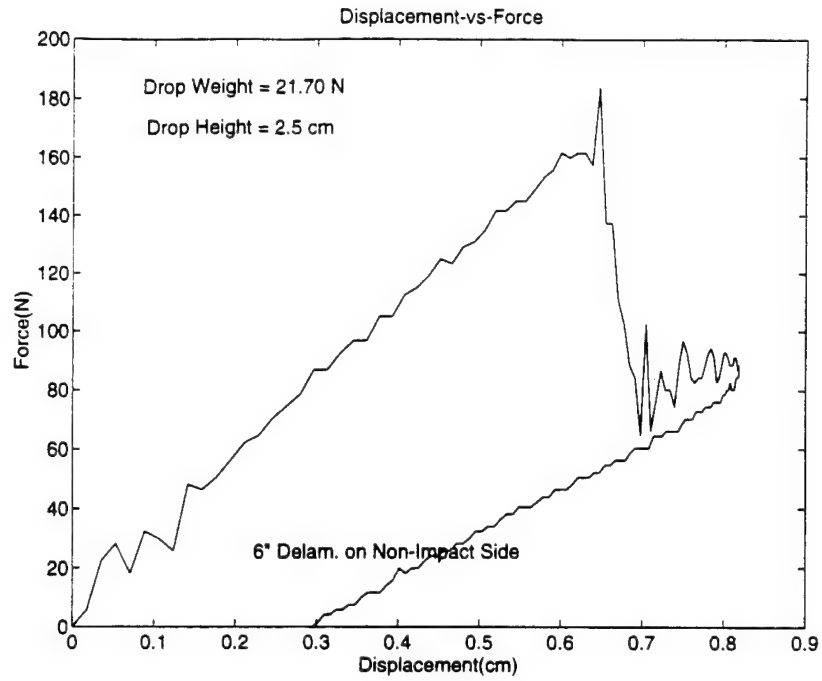




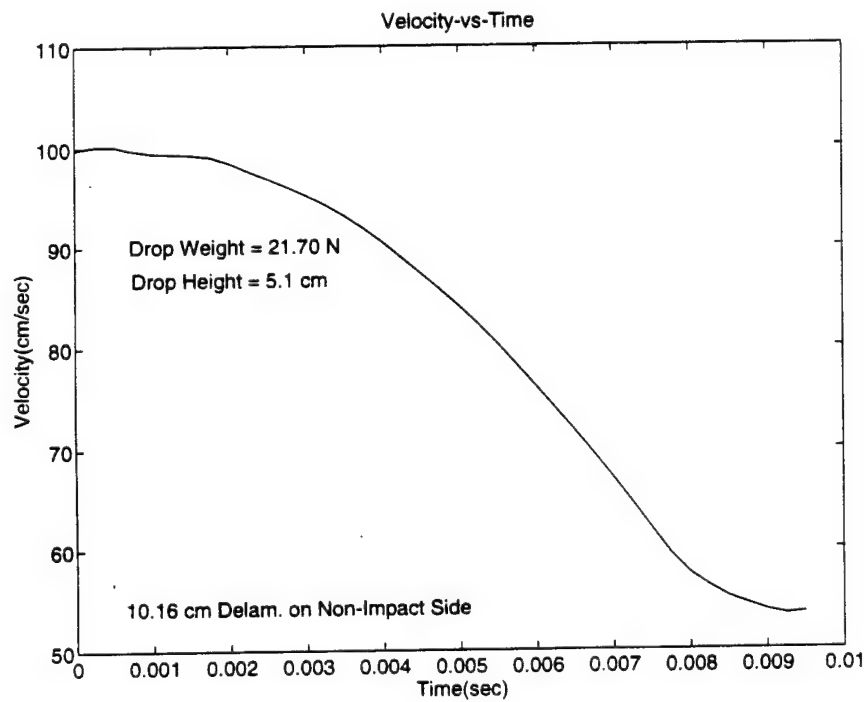
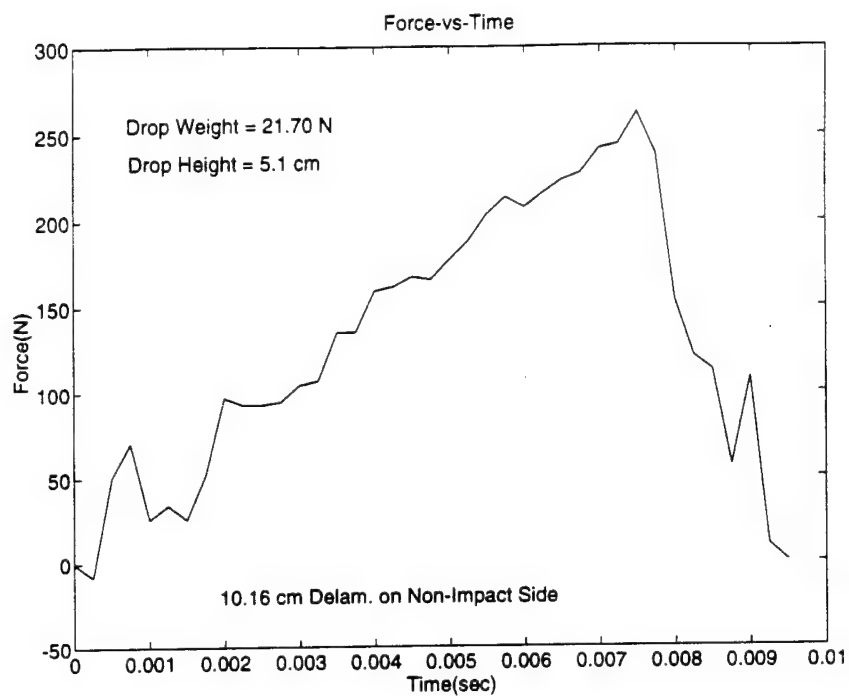


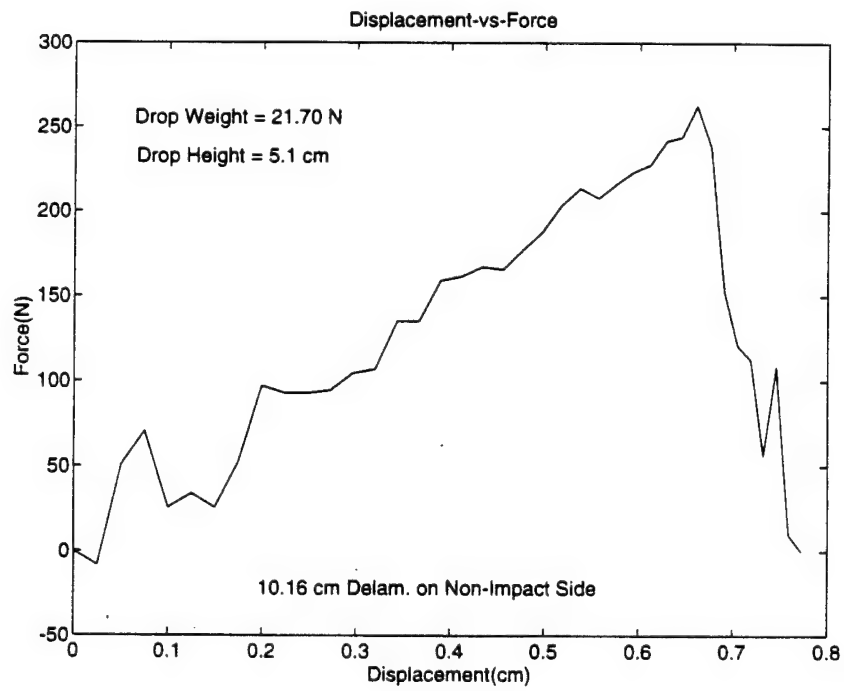
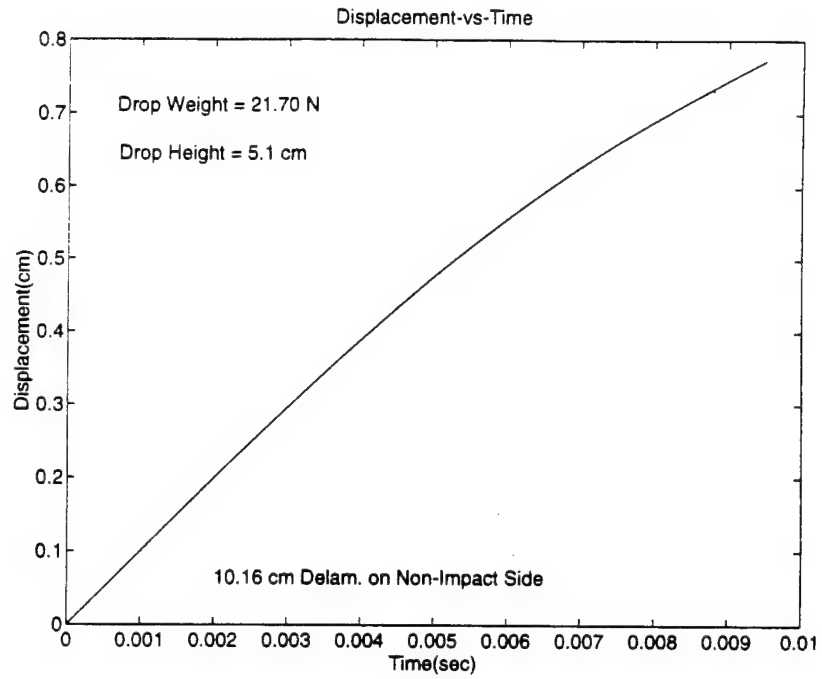


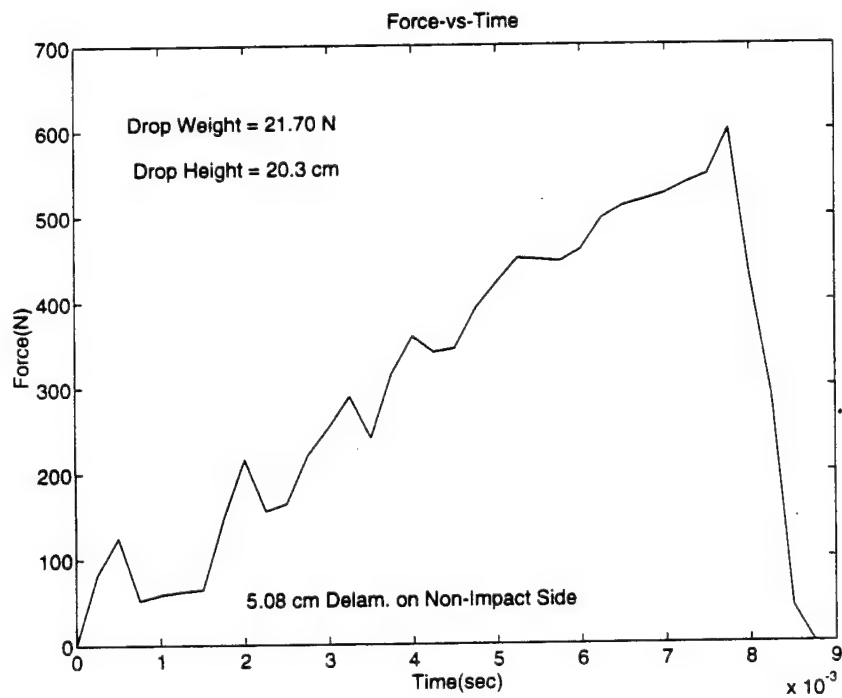
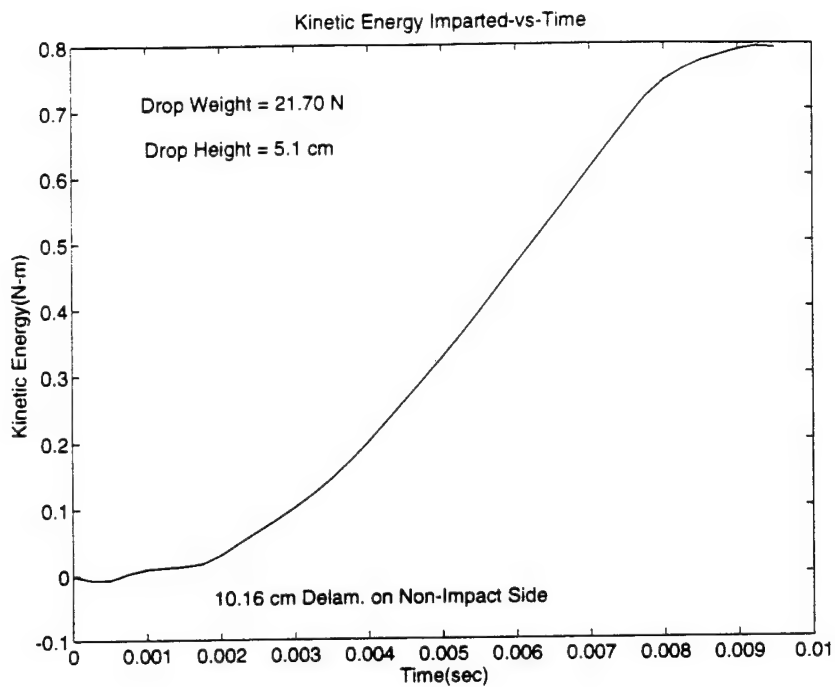


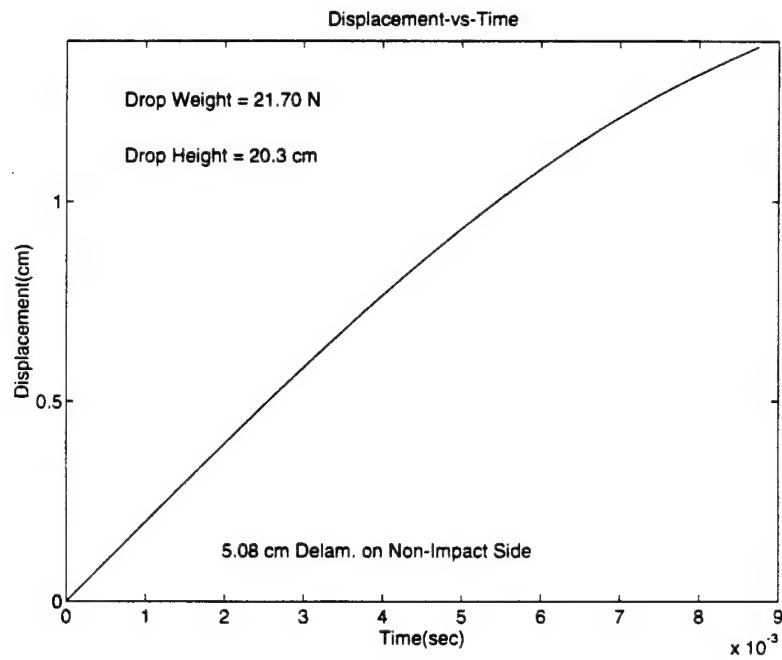
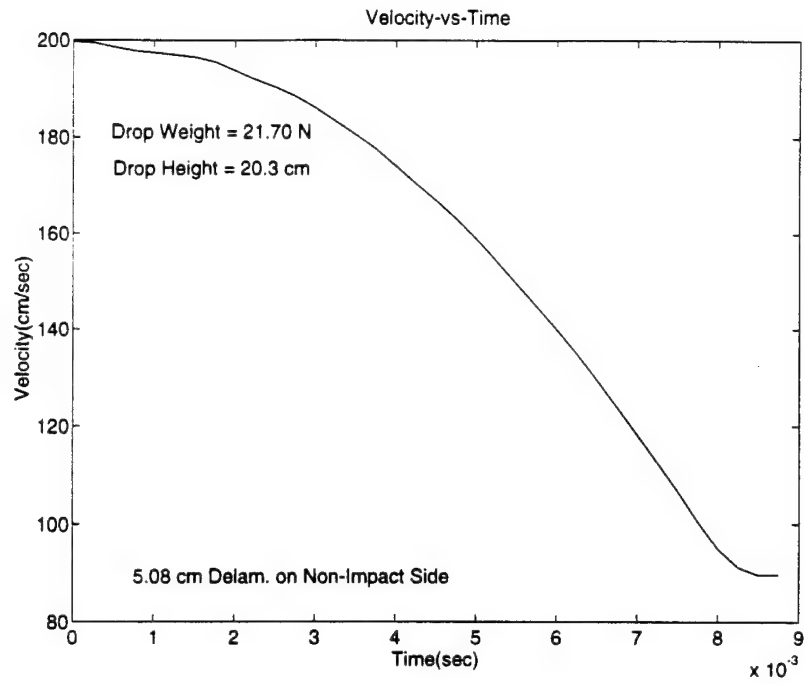


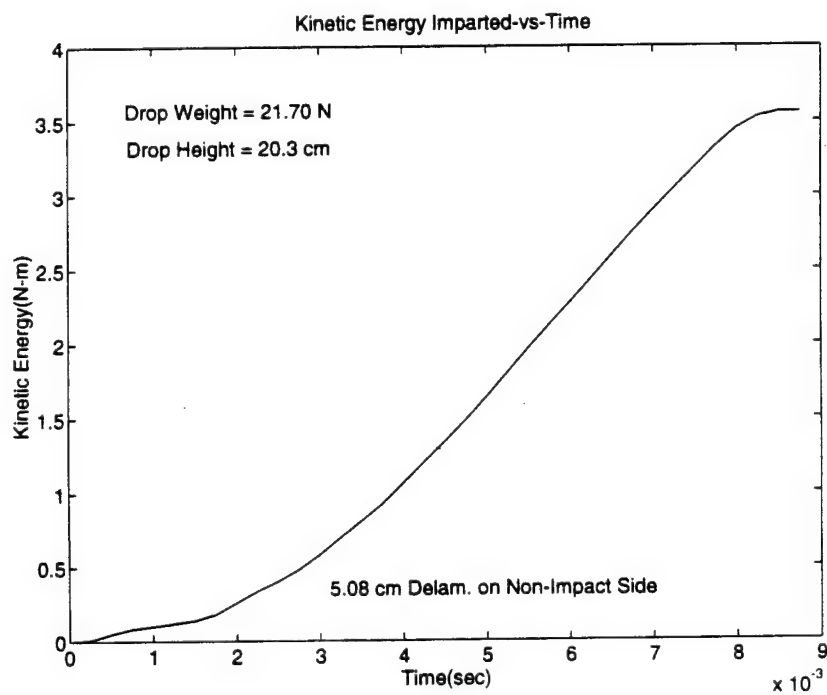
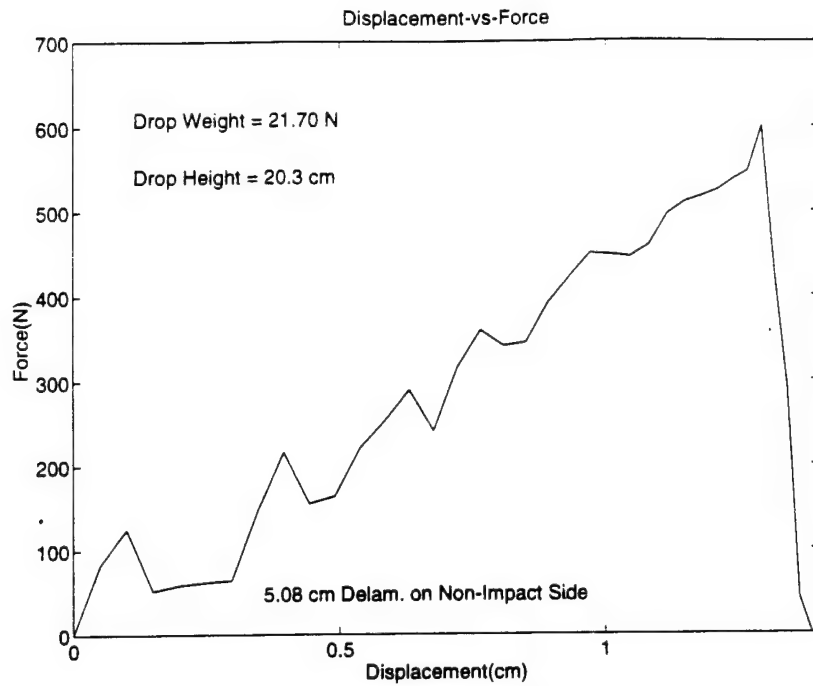


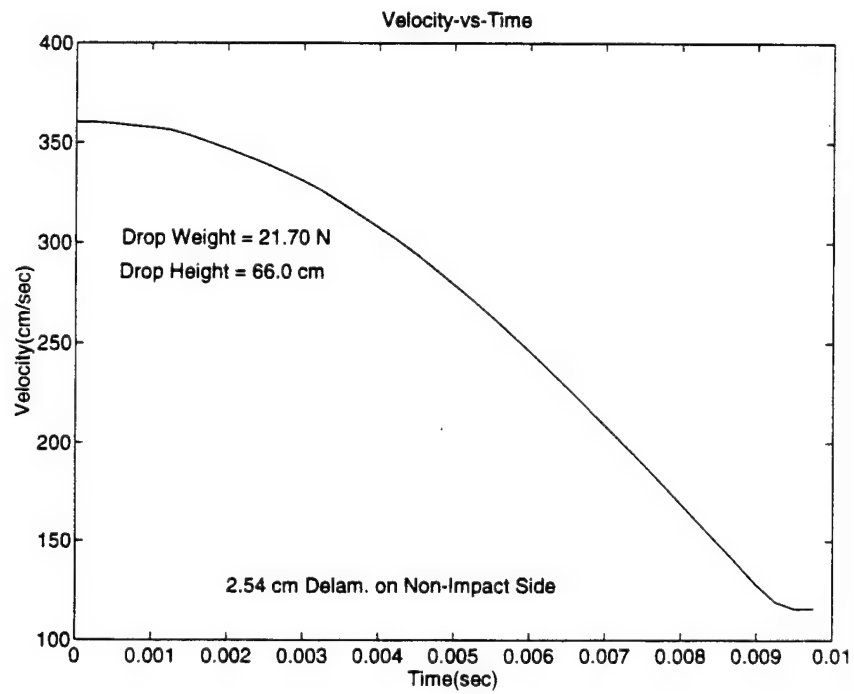
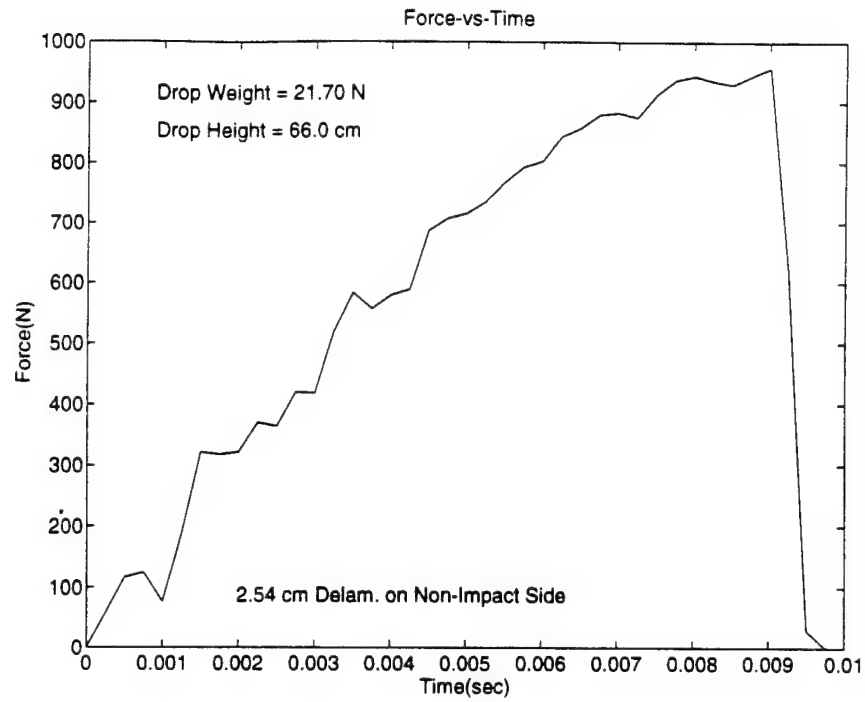


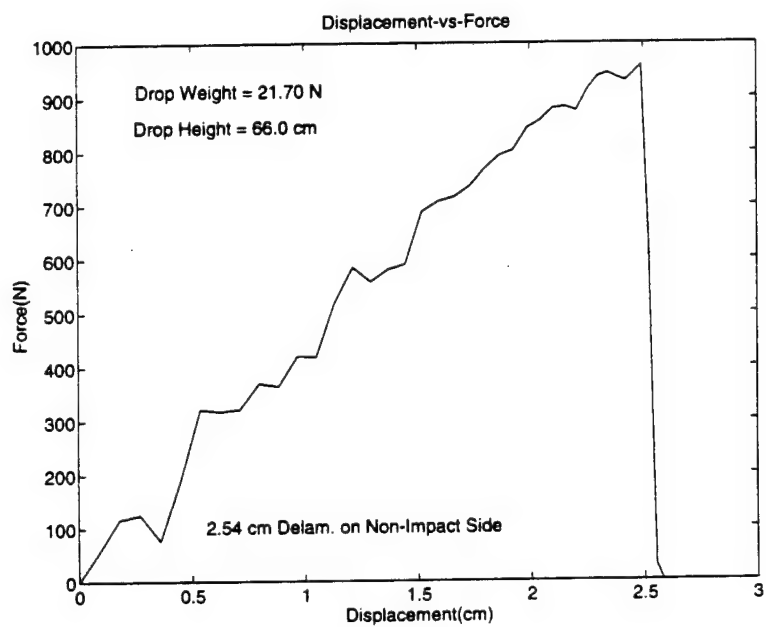
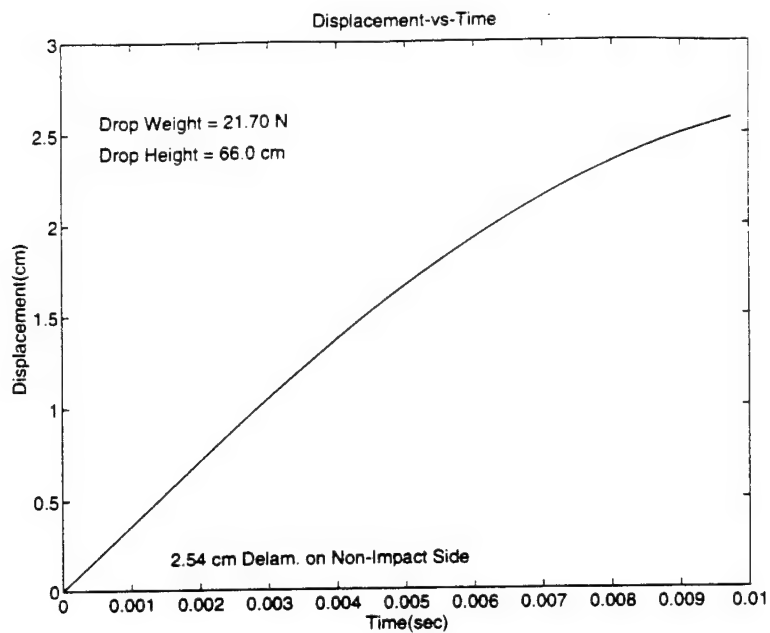


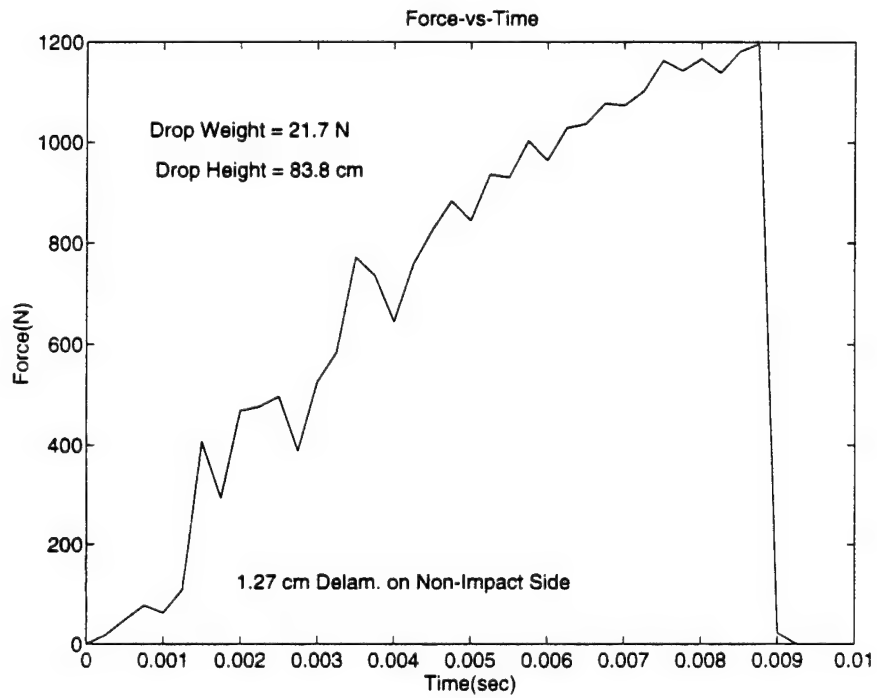
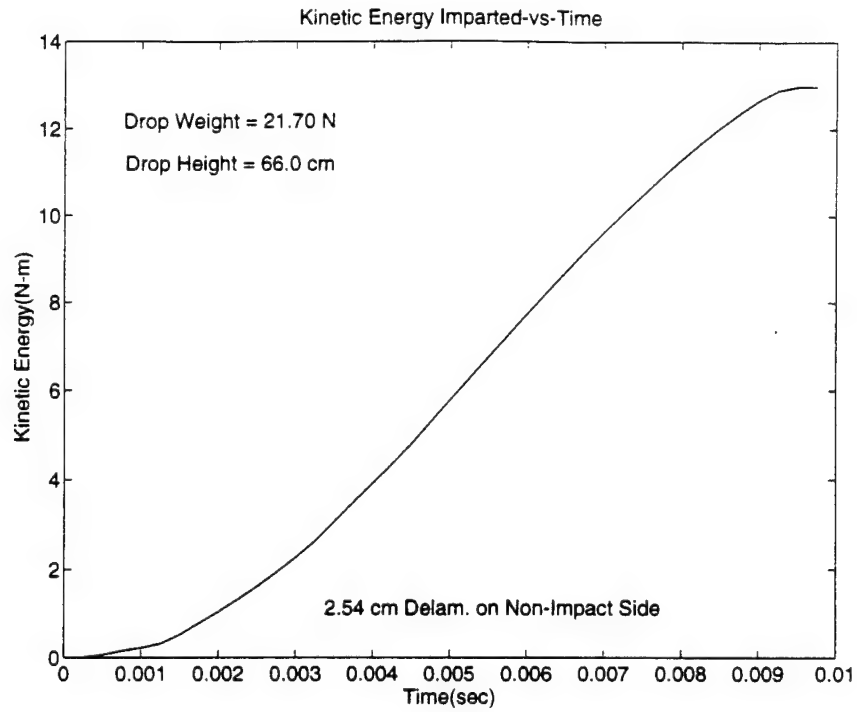




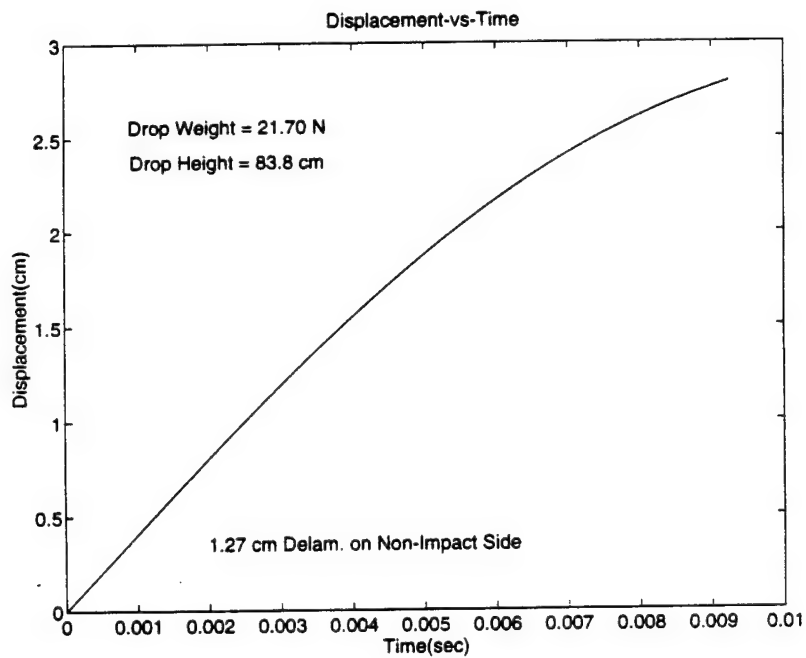
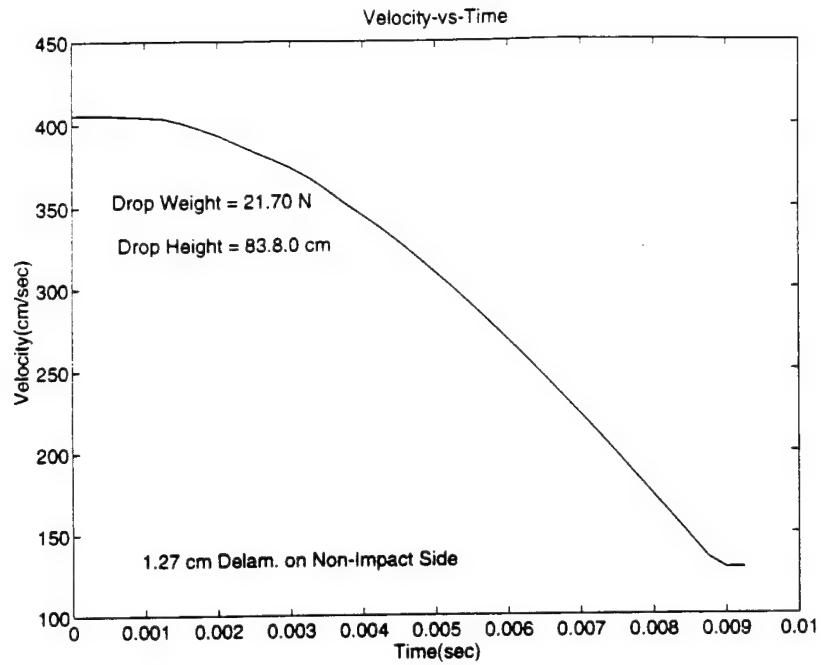


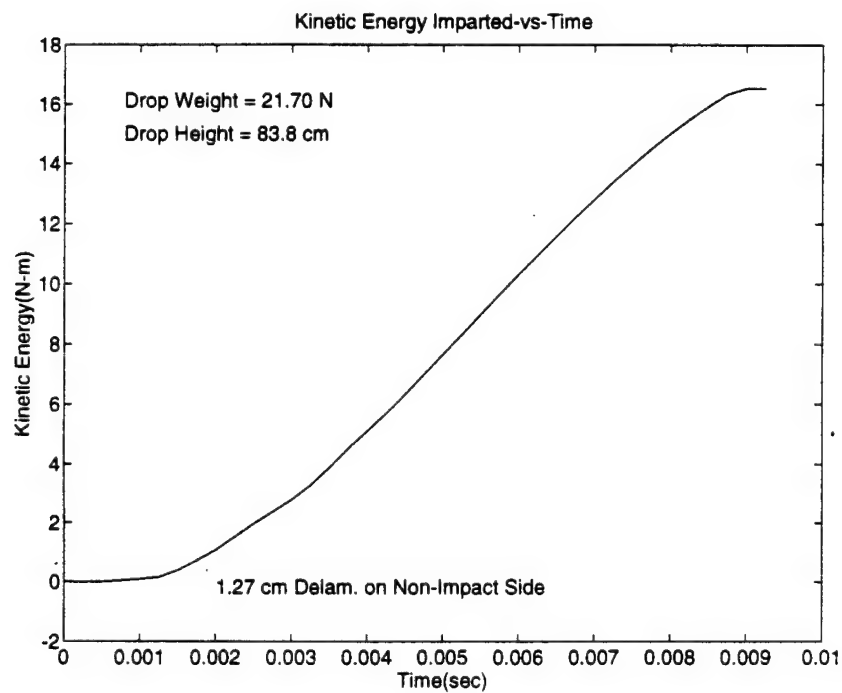
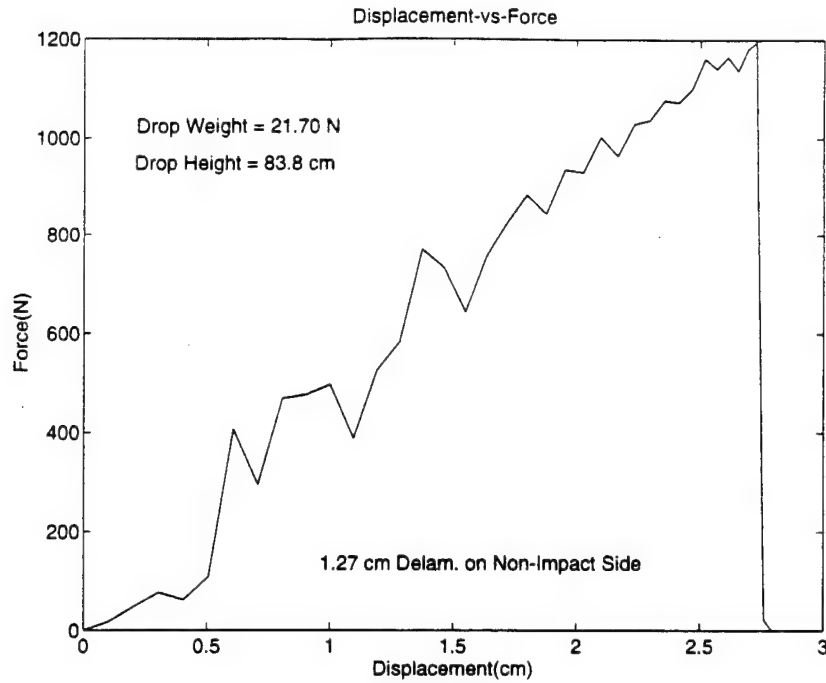


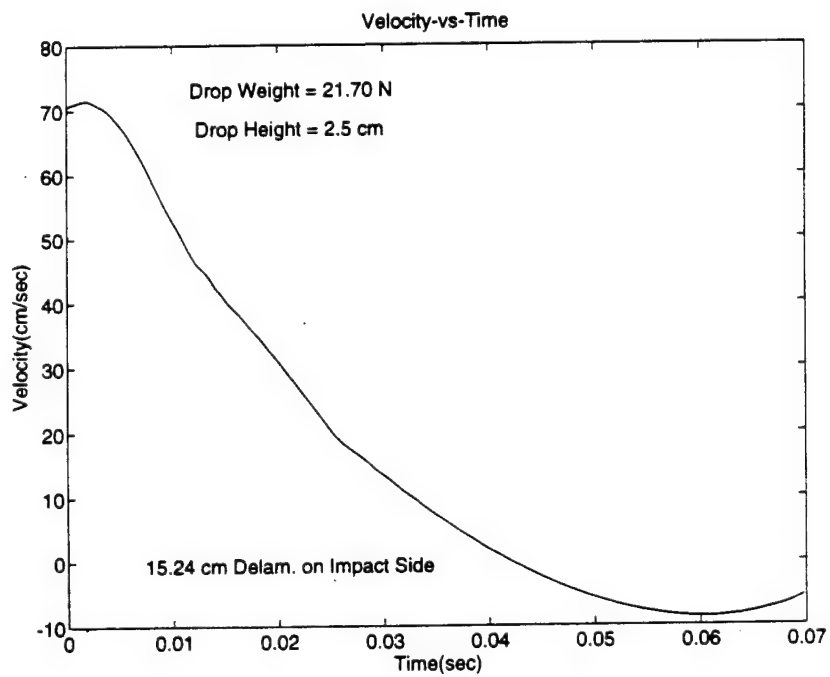
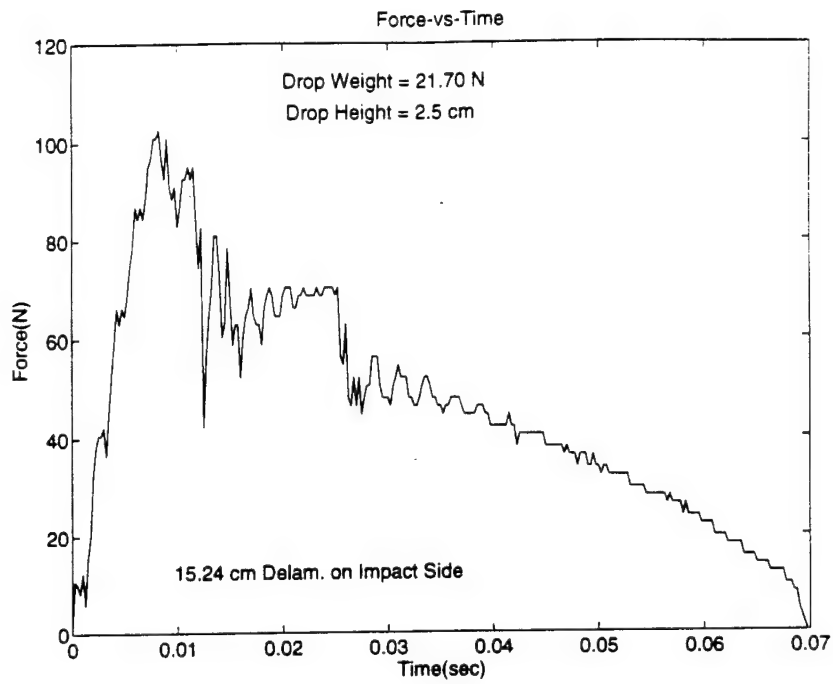


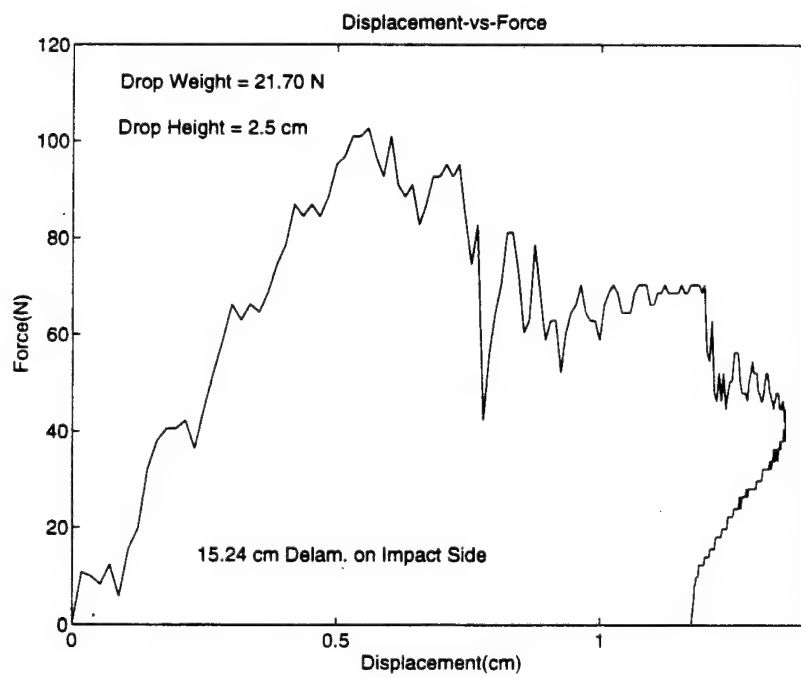
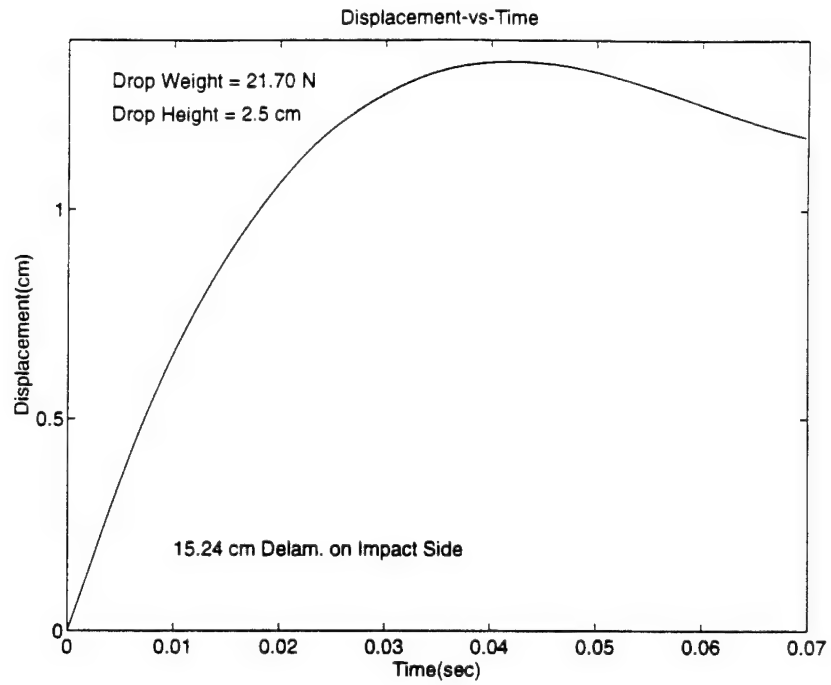


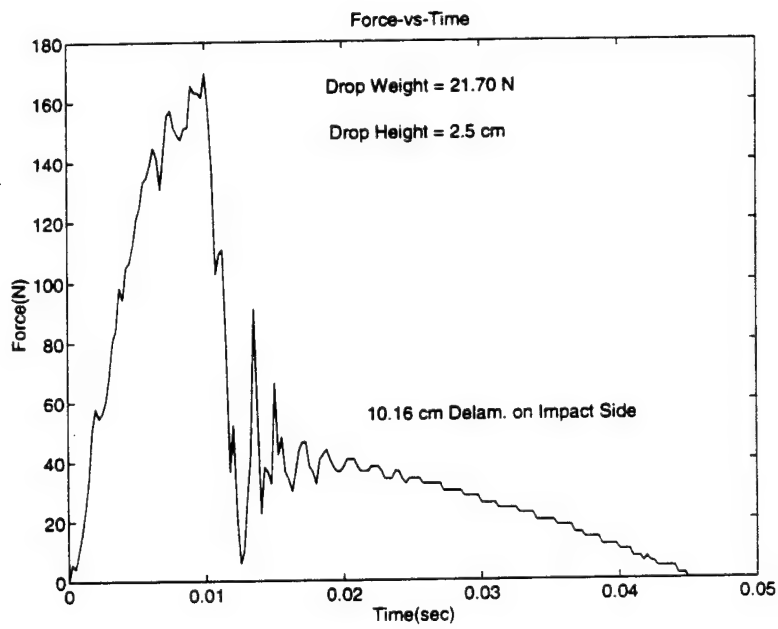
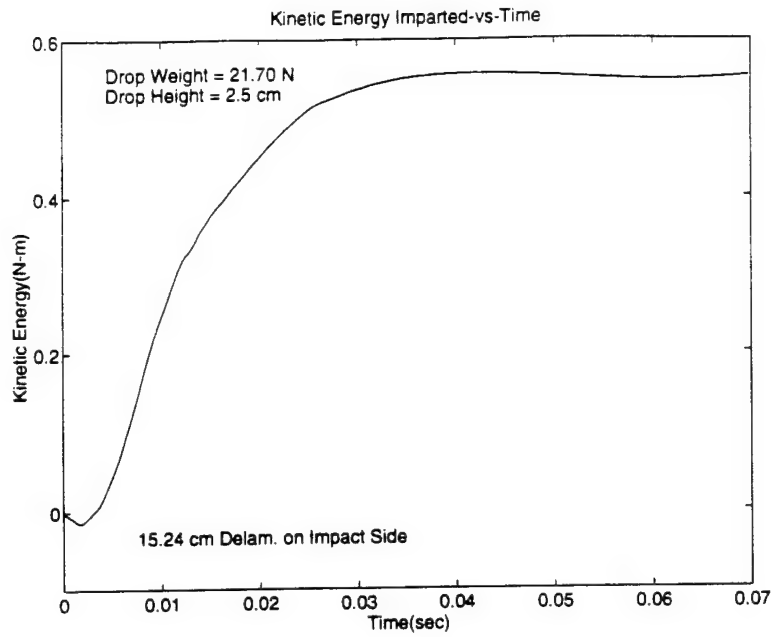


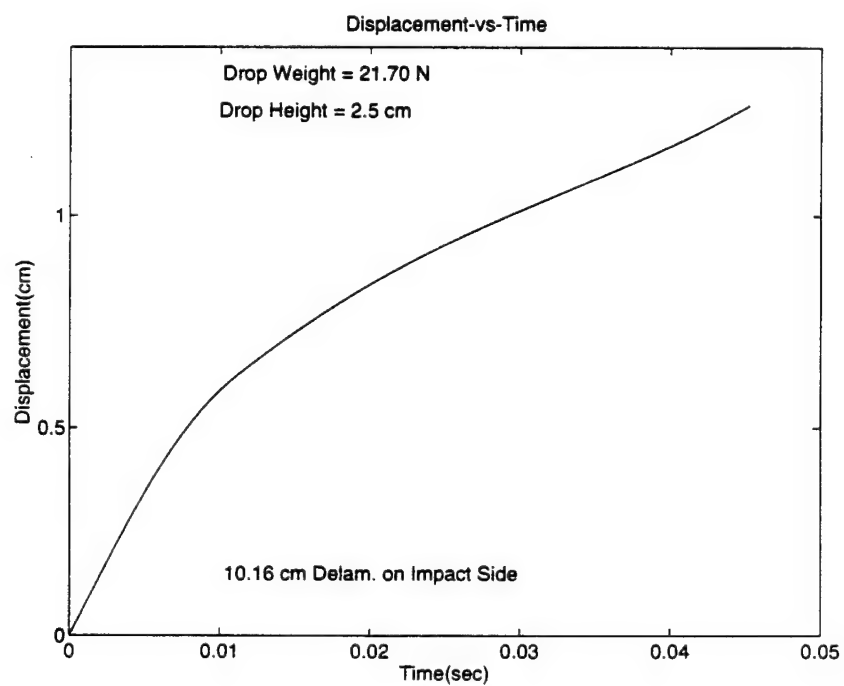
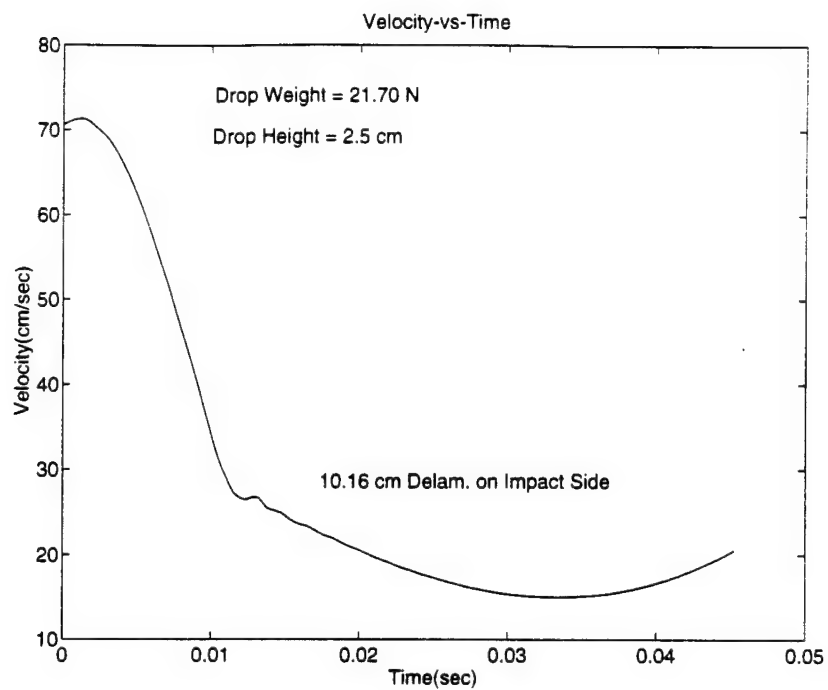


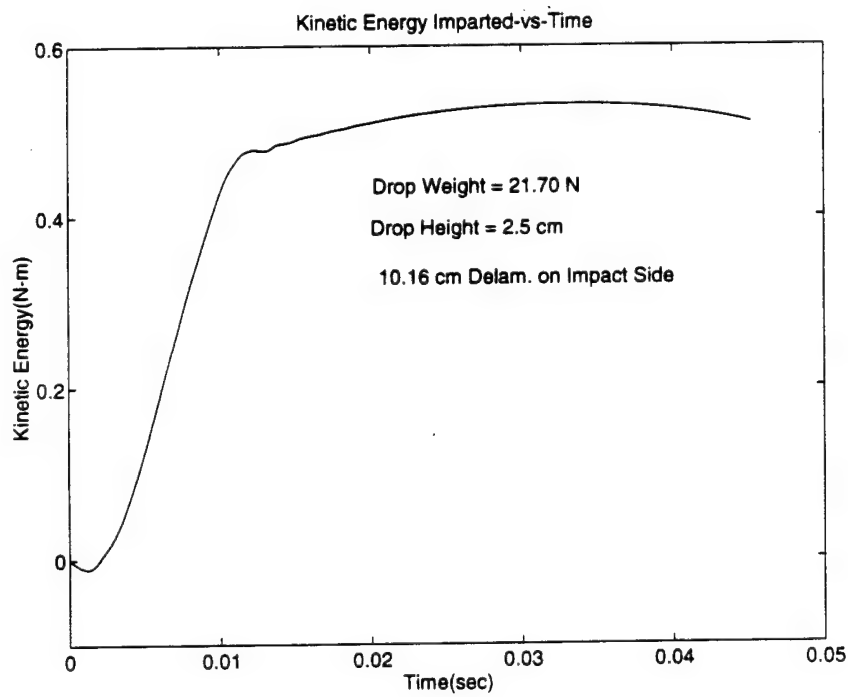
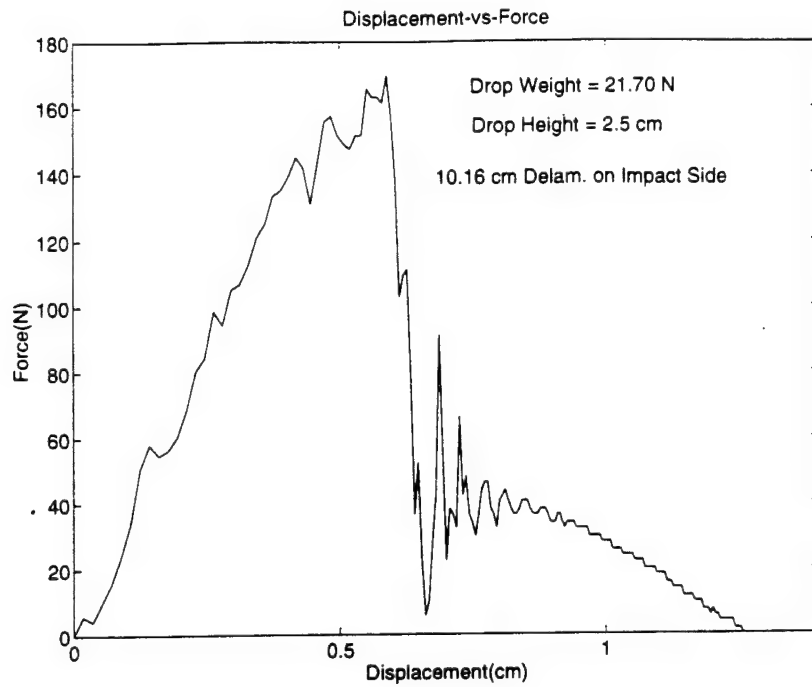


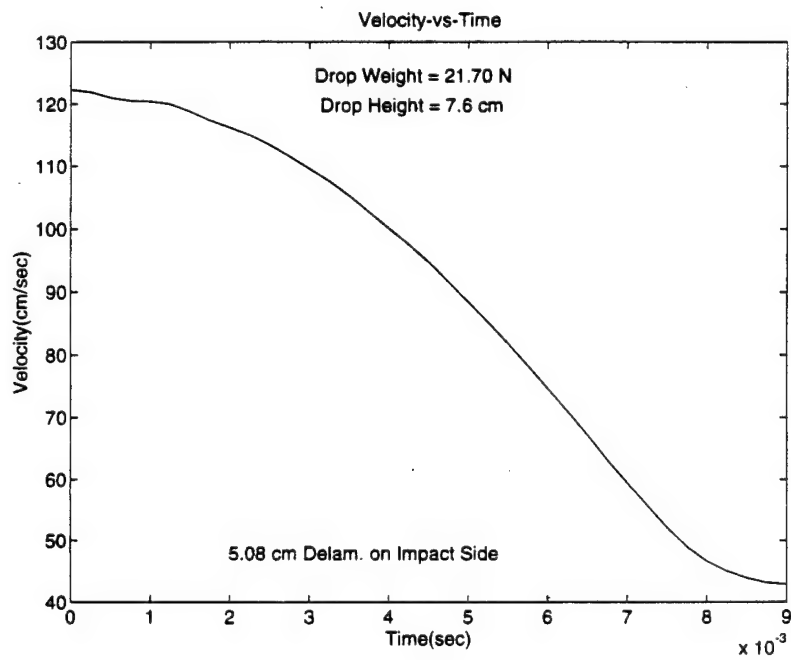
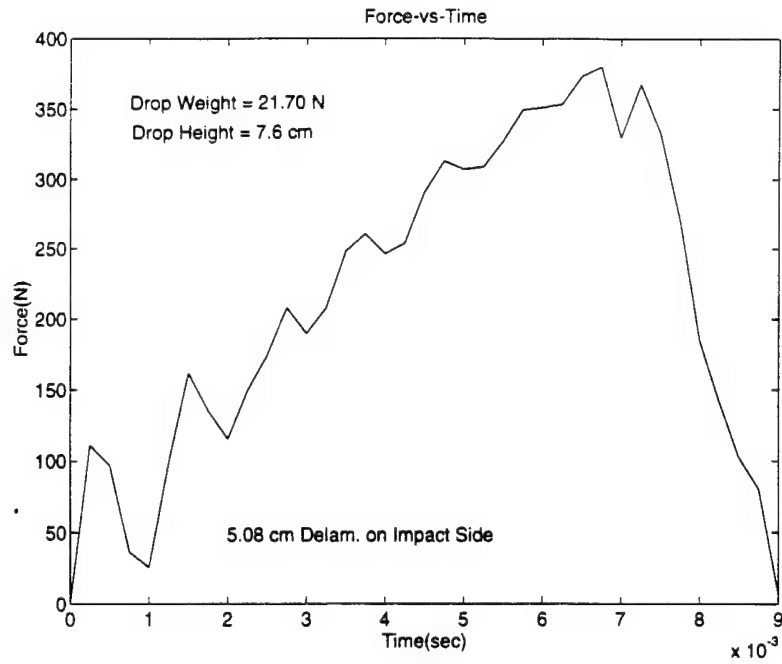




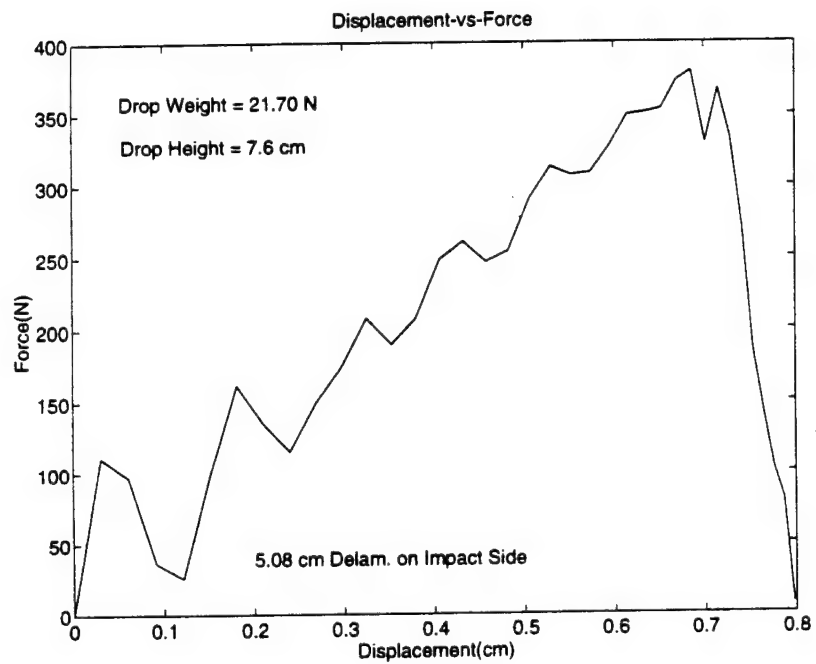
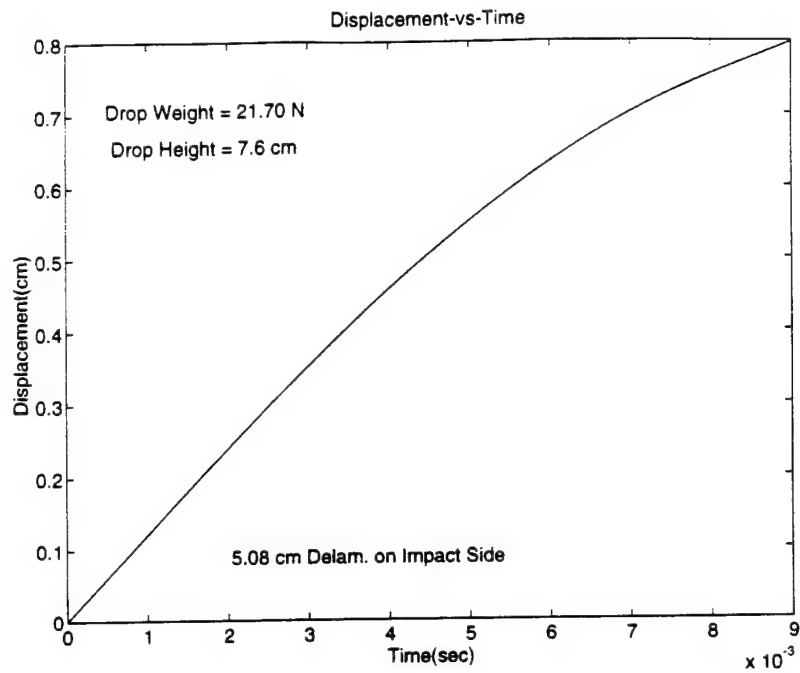


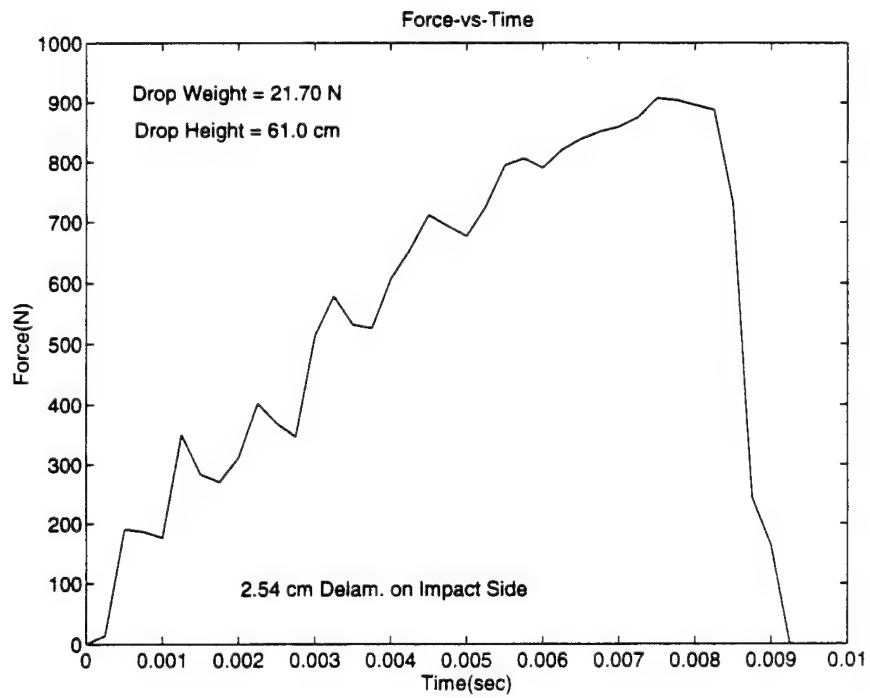
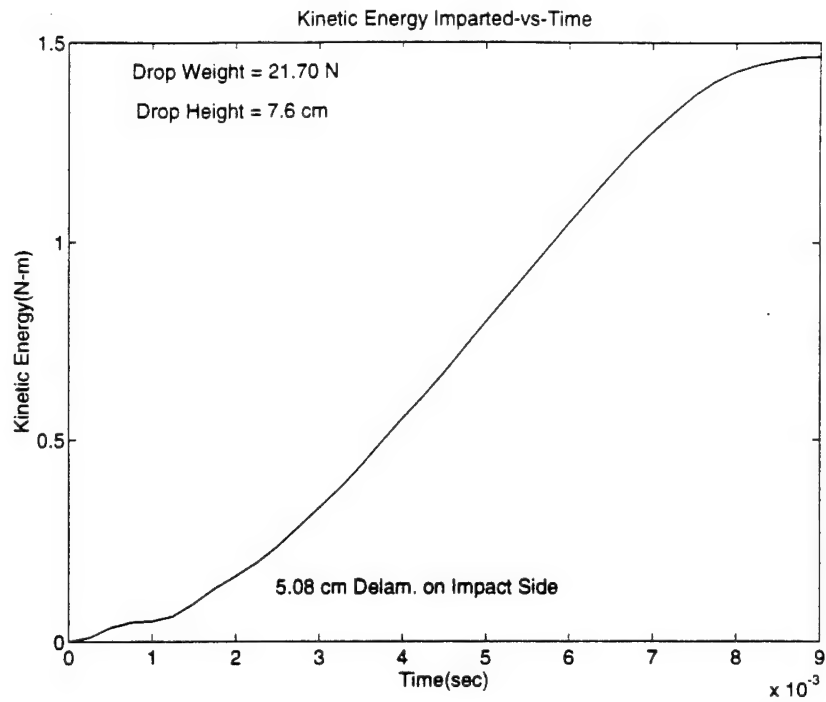


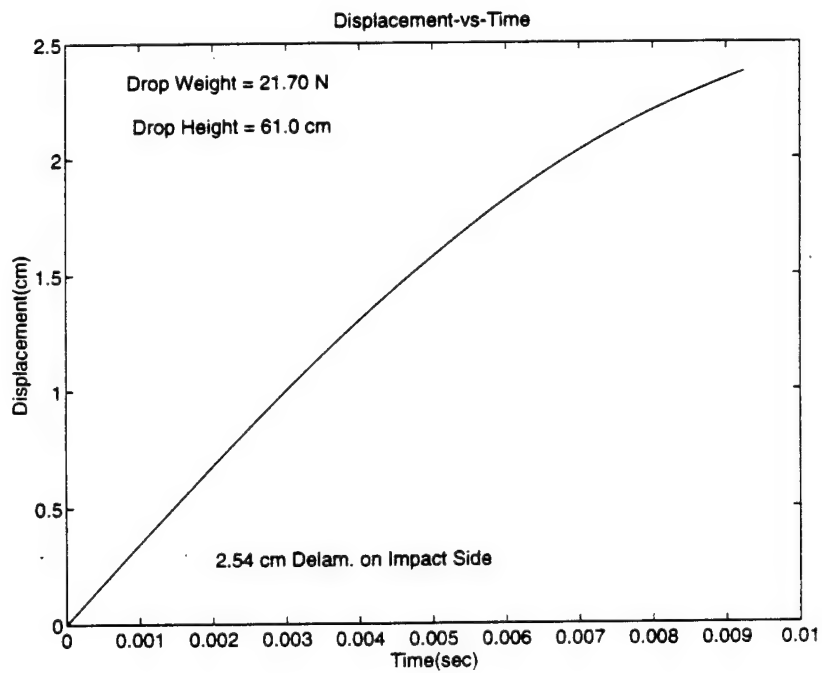
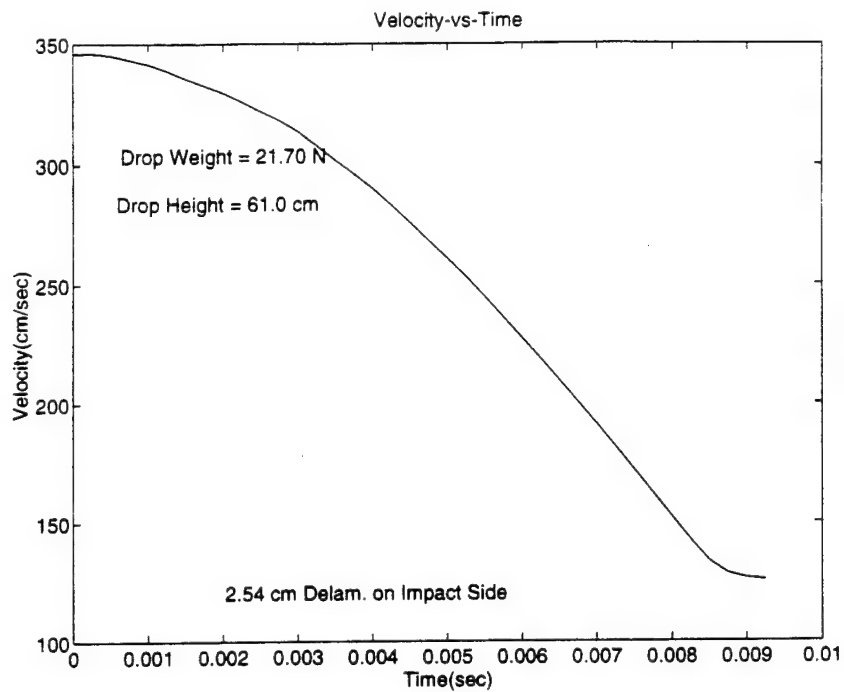


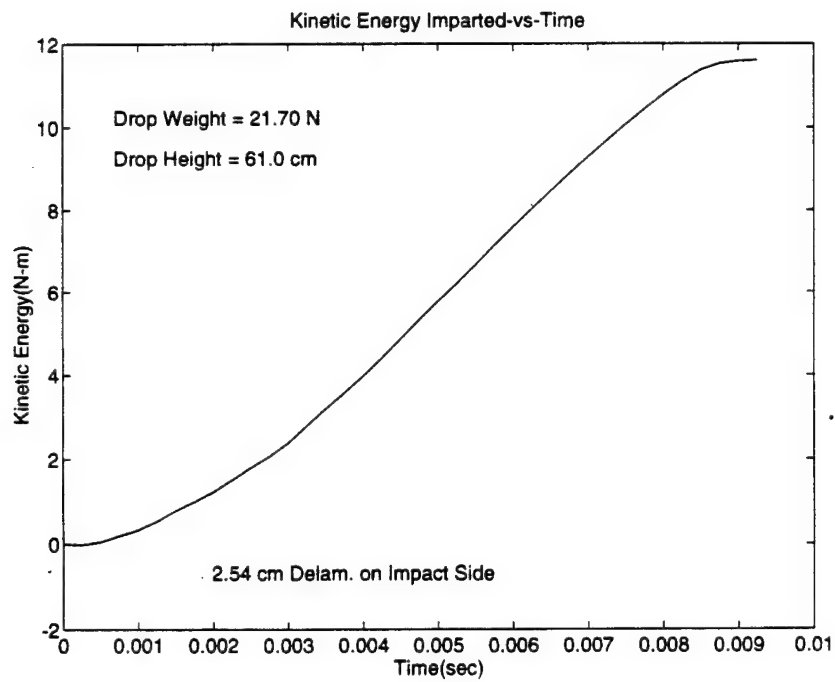
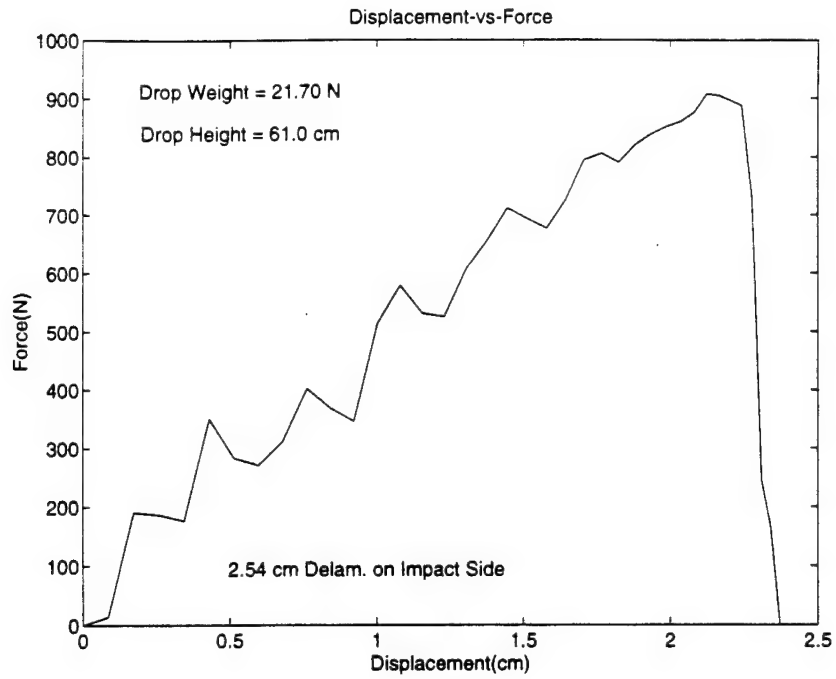


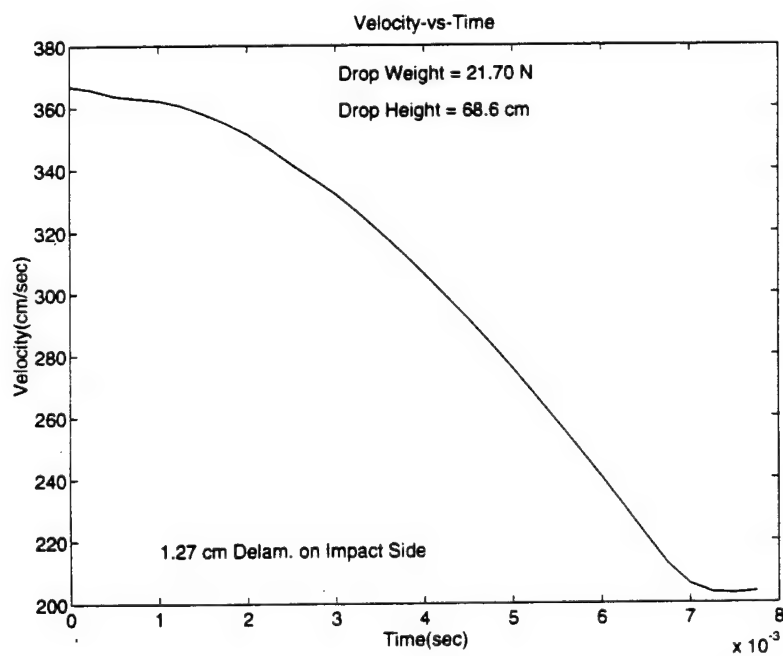
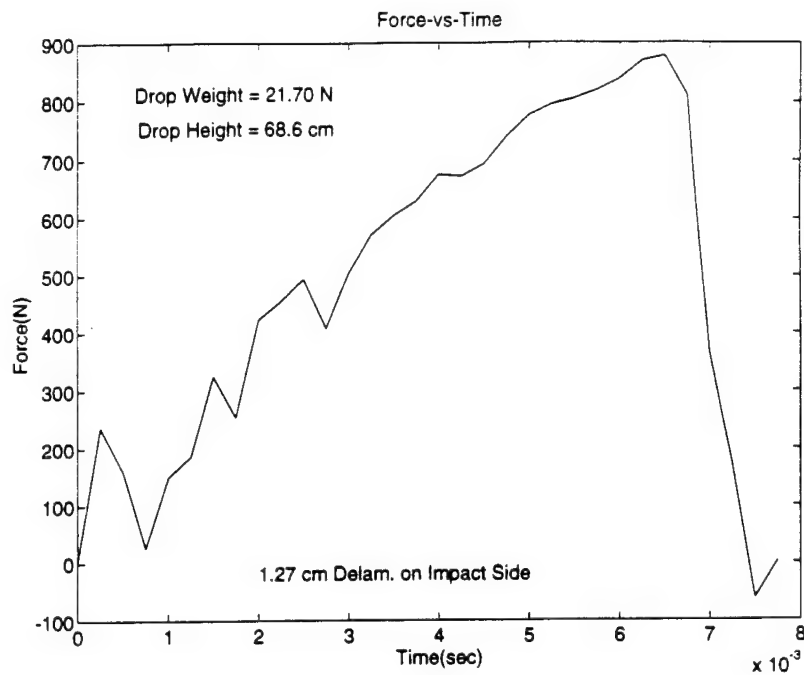


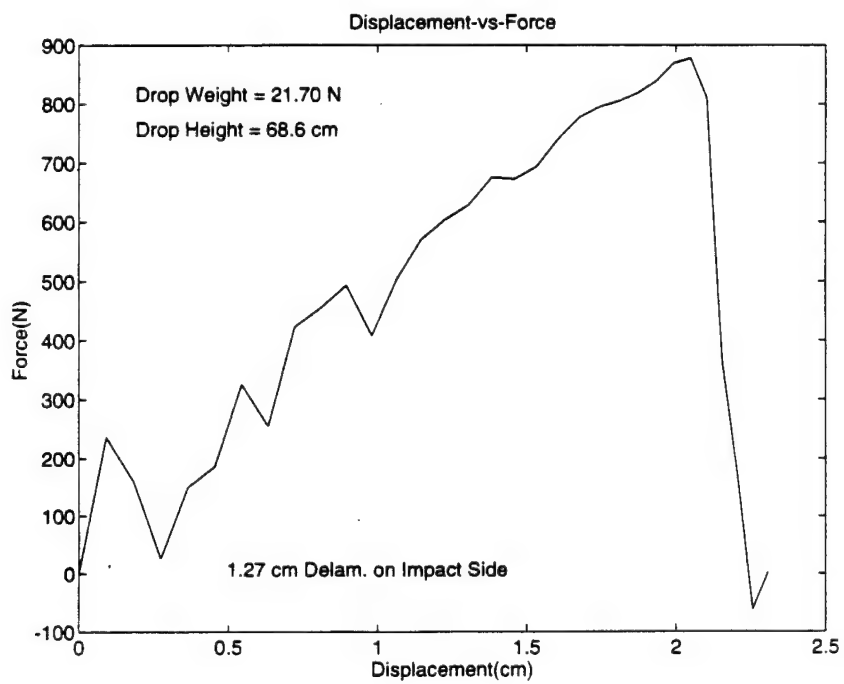
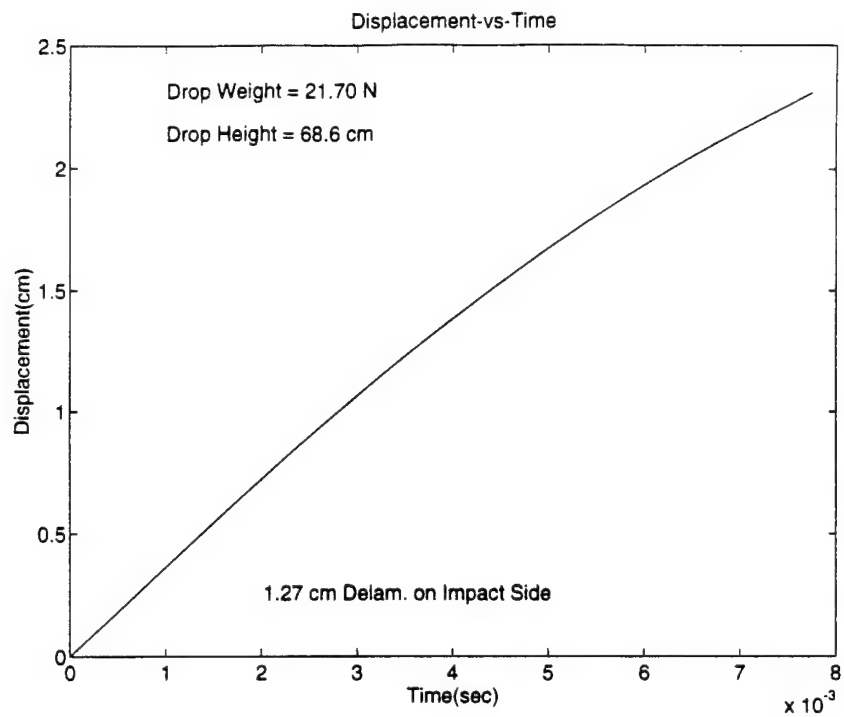


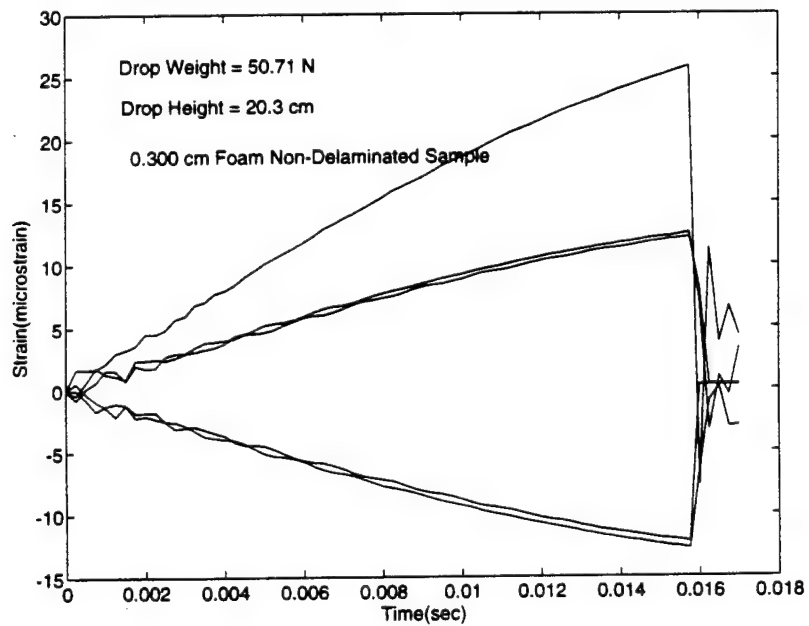
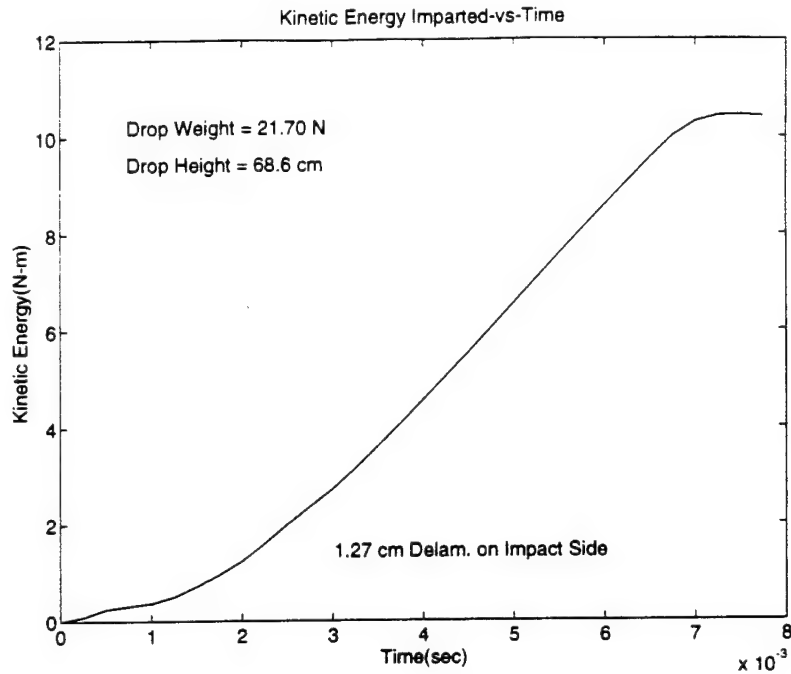


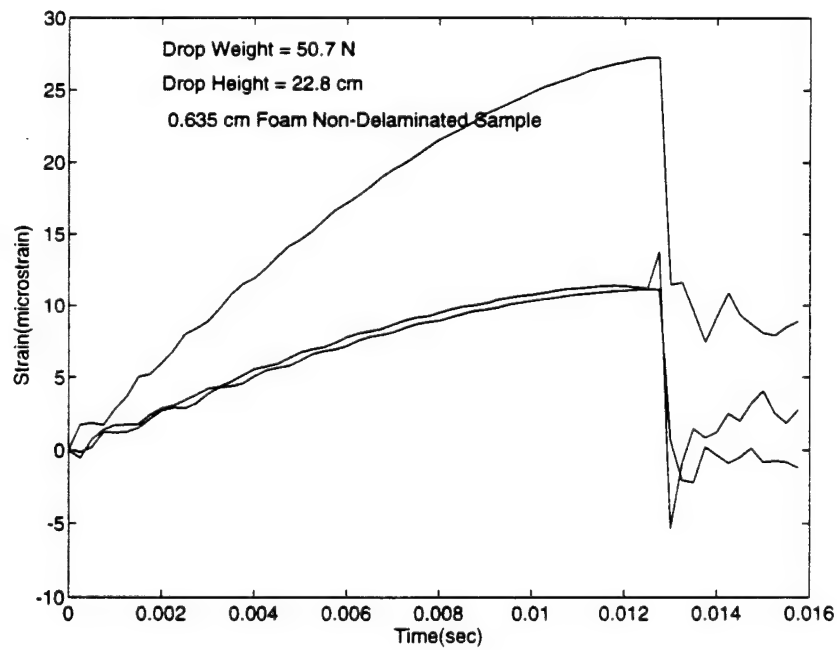
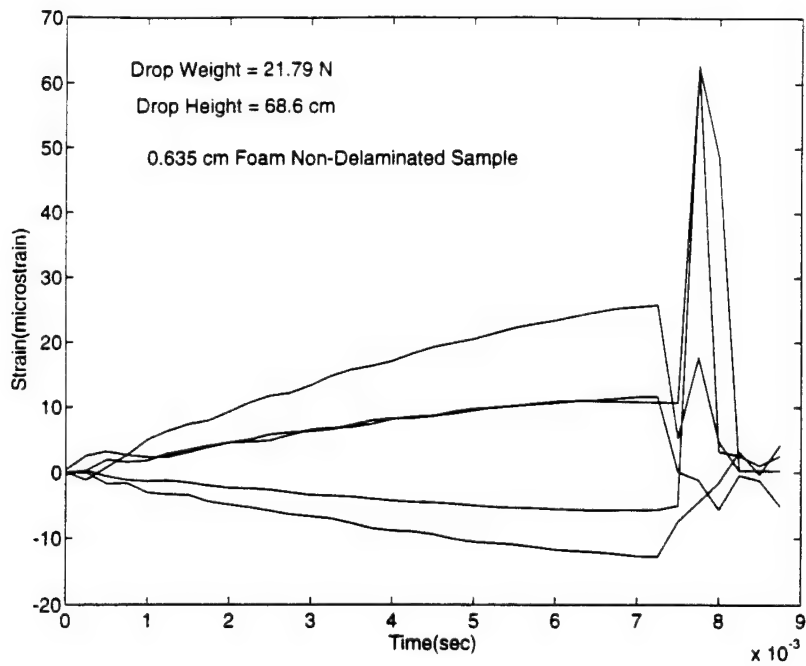




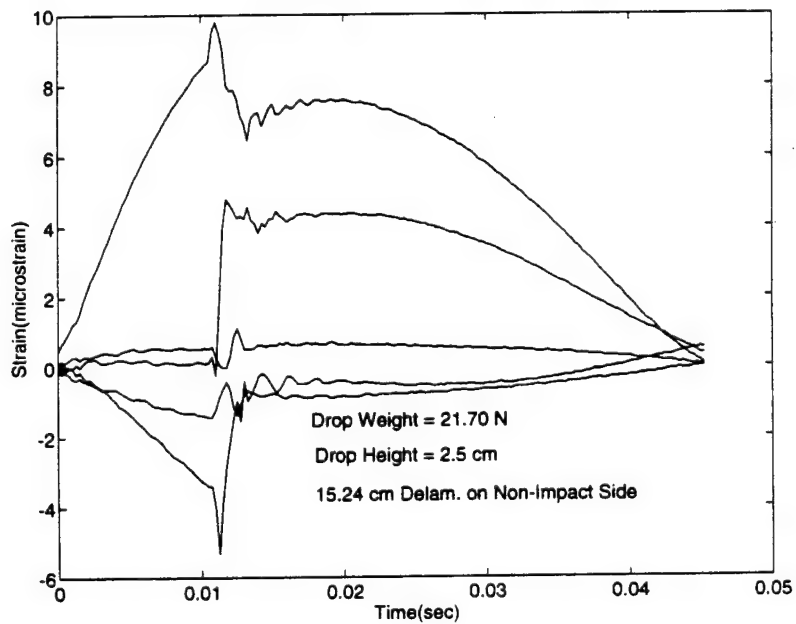
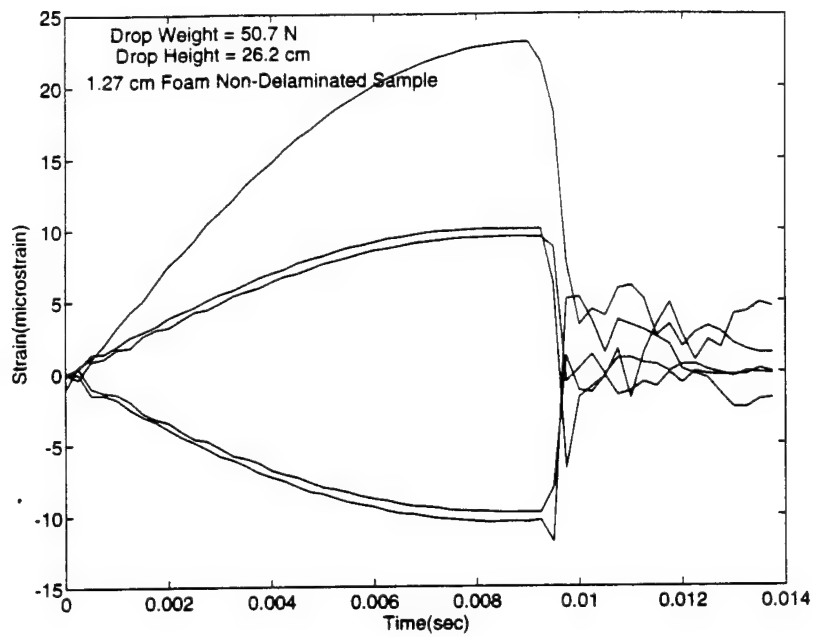


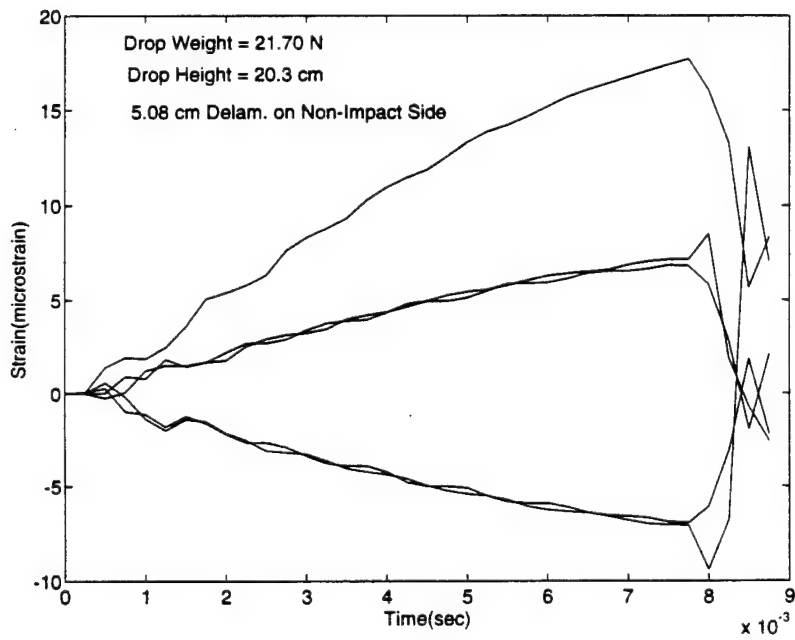
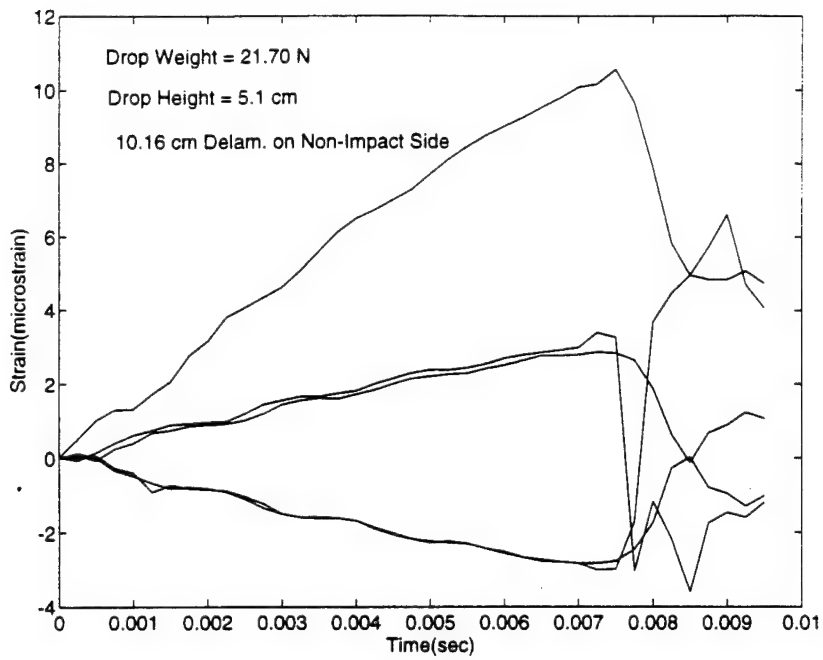


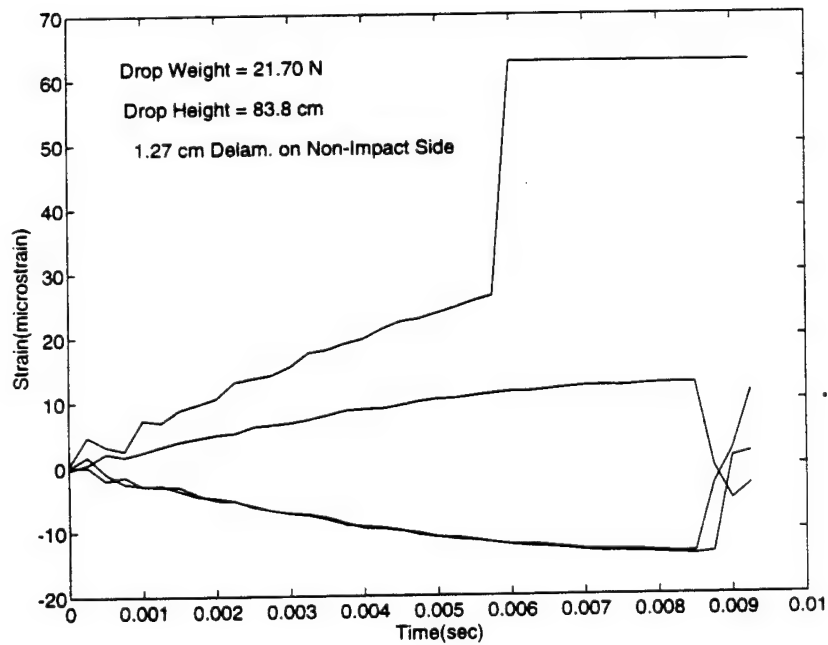
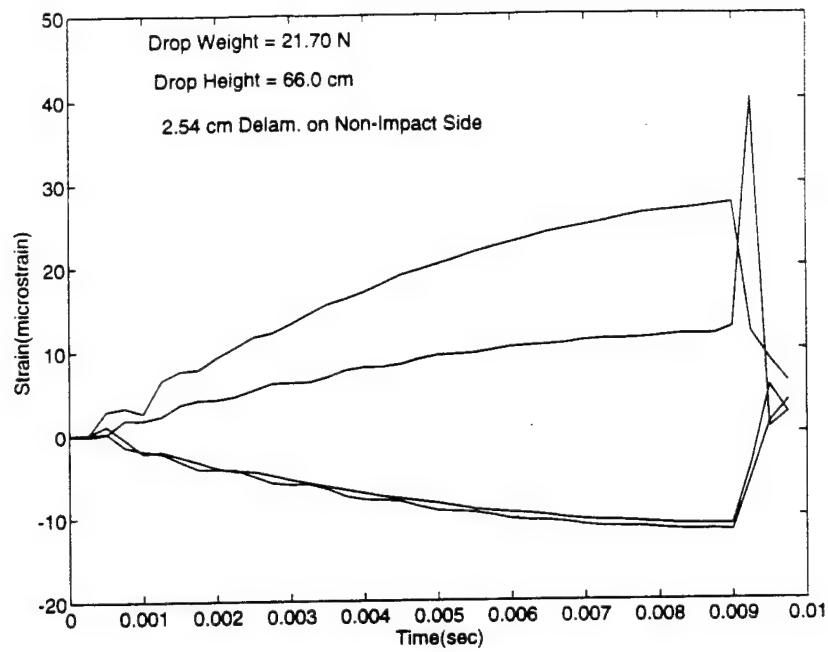


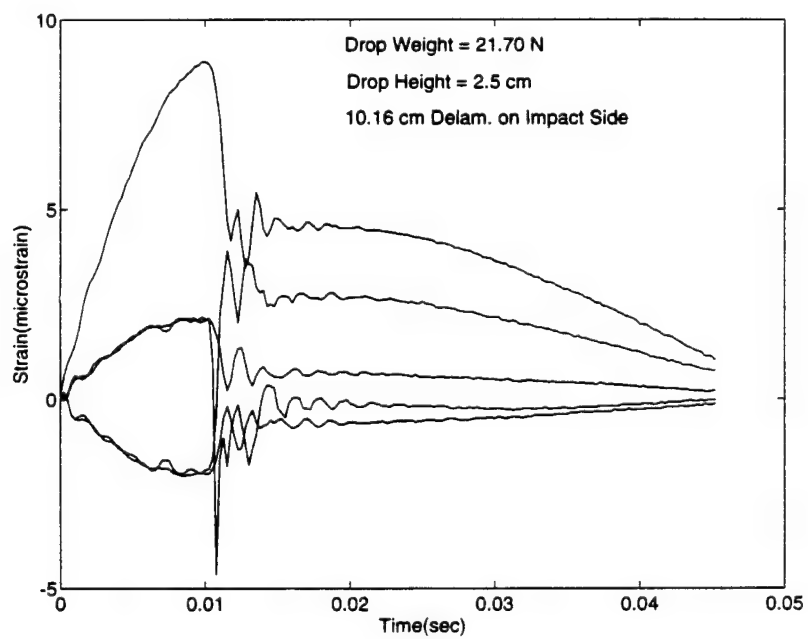
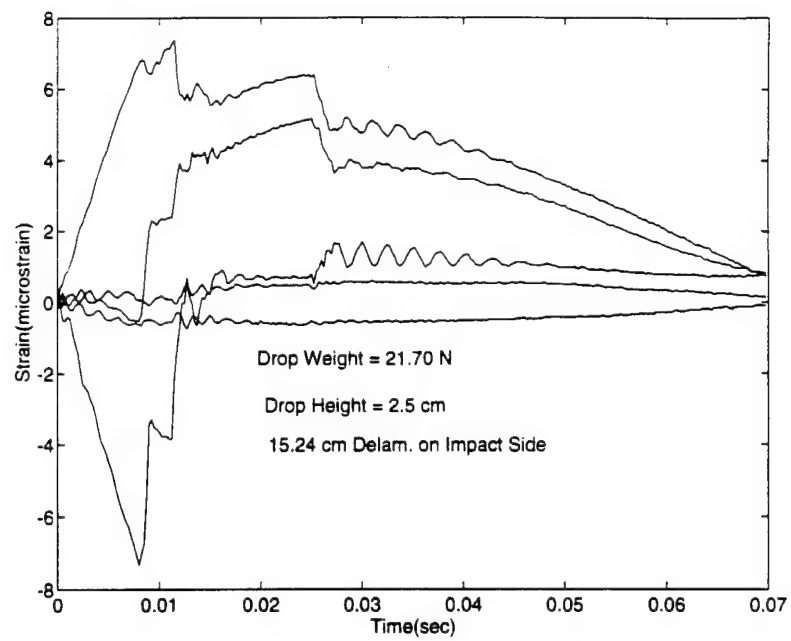


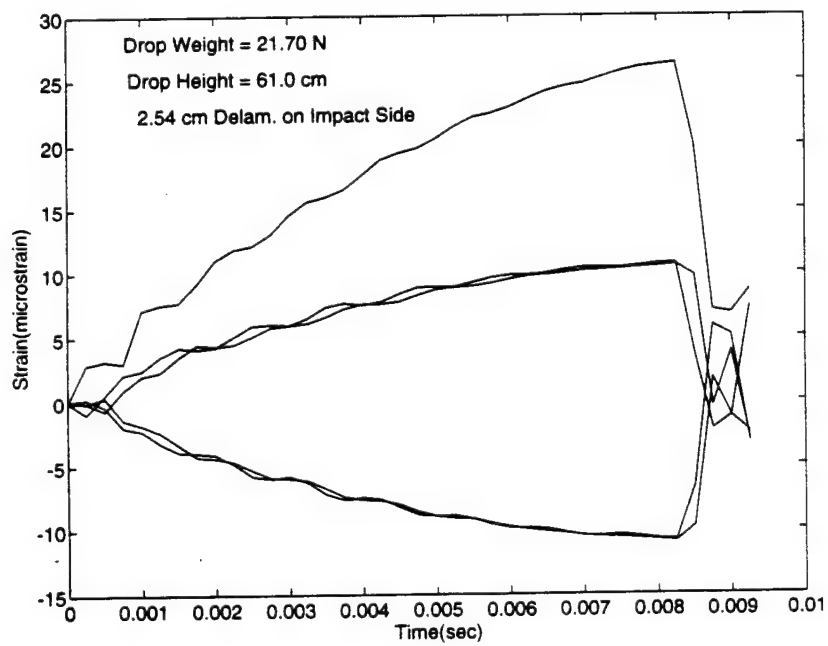
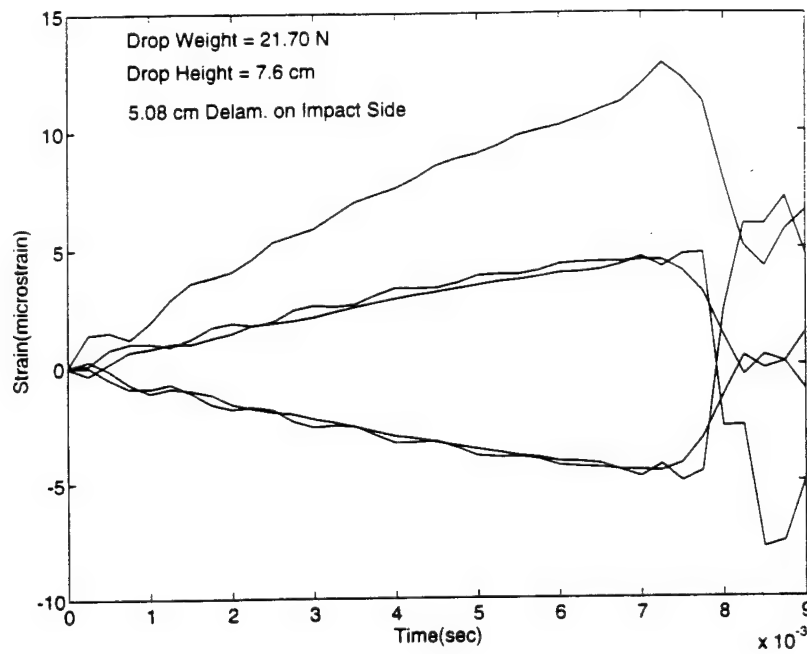


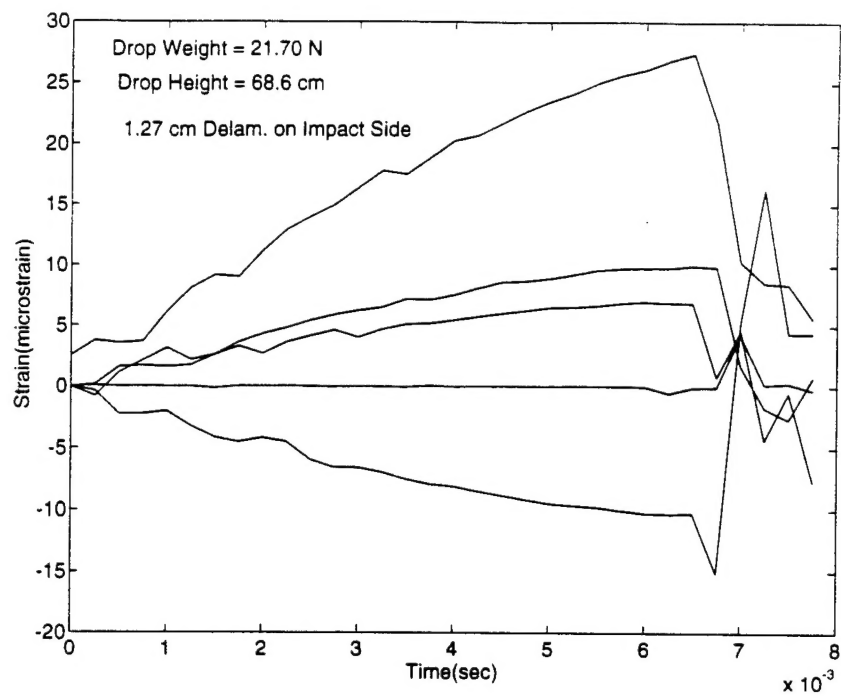












## LIST OF REFERENCES

1. David Taylor Research Center, DTRC-SME-88/73, *INSTRUMENTED IMPACT TESTING OF COMPOSITE MATERIALS*, by R. M. Crane and T. D. Juska, January 1989.
2. Nemes, J. A., and Simmonds, K. E., (1992) "Low-Velocity Impact Response of Foam-Core Sandwich Composites," *Journal of Composite Materials*, 26, 4.
3. Kim, C., and Jun, E., (1992) "Impact Resistance of Composite Laminated Sandwich Plates," *Journal Of Composite Materials*, 26, 15.
4. Shi, Y. B., and Hull, D., (1992) "Fracture of Delaminated Unidirectional Composite Beams," *Journal of Composite Materials*, 26, 15.
5. Sjoblom, P. O., Hartness, J. T., and Cordell, T. M., (1988) "On Low-Velocity Impact Testing of Composite Materials," *Journal of Composite Materials*, 22, January.
6. Carlyle, J. D., and Adler, W. F., *Damage Tolerance Assessment Procedures for Composite Materials and Components*, presented at the JANNAF Composite Motor Case Subcommittee/Structures and Mechanical Behavior Subcommittee Joint Meeting. Pasadena, California (November 27-30, 1984).
7. Jea, L. C., and Felbeck, D. k., (1980) "Increased Fracture Toughness of Graphite-Epoxy Composites through Intermittent Interlaminar Bonding," *Journal of Composite Materials*, 14, January.
8. Hwu, C., and Hu, J. S., (1992) "Buckling and Postbuckling of Delaminated Composite Sandwich Beams," *American Institute of Aeronautics and Astronautics*, 30, 7.





# INITIAL DISTRIBUTION LIST

	No. Copies
1. Defense Technical Information Center Cameron Station Alexandria VA 22304-6145	2
2. Library, Code 052 Naval Postgraduate School Monterey CA 93943-5101	2
3. Professor Y. W. Kwon, Code ME/Kw Department of Mechanical Engineering Naval Postgraduate School Monterey CA 93943-5000	2
4. Department Chairman, Code ME/Kk Department of Mechanical Engineering Naval Postgraduate School Monterey CA 93943-5000	1
5. Naval Engineering Curricular Office, Code 34 Naval Postgraduate School Monterey CA 93943-5000	1
6. Mr. David Bonnani Naval Surface Warfare Center, Carderock Div Code 1720.2 Bethesda MD 20084-5000	1
7. Lt. L. A. Clawson, Jr Puget Sound Naval Shipyard Bremerton WA 98314-5001	2
8. Dr. Joseph Corrado Naval Surface Warfare Center Carderock Division Code 011 Bethesda, MD 20084-5000	1
9. Mr. Erik A. Rasmussen Naval Surface Warfare Center Carderock Division Code 1720.4 Brthesda, MD 20084-5000	1